Metal-based multihelicenic architectures

Etienne S. Gauthier, Rafael Rodríguez-Muñoz, Jeanne Crassous

10.1002/anie.202004361

WILEY-VCH

MINIREVIEW

Metal-based multihelicenic architectures

Etienne S. Gauthier,† Rafael Rodríguez † and Jeanne Crassous*[a]

Dedication ((optional))

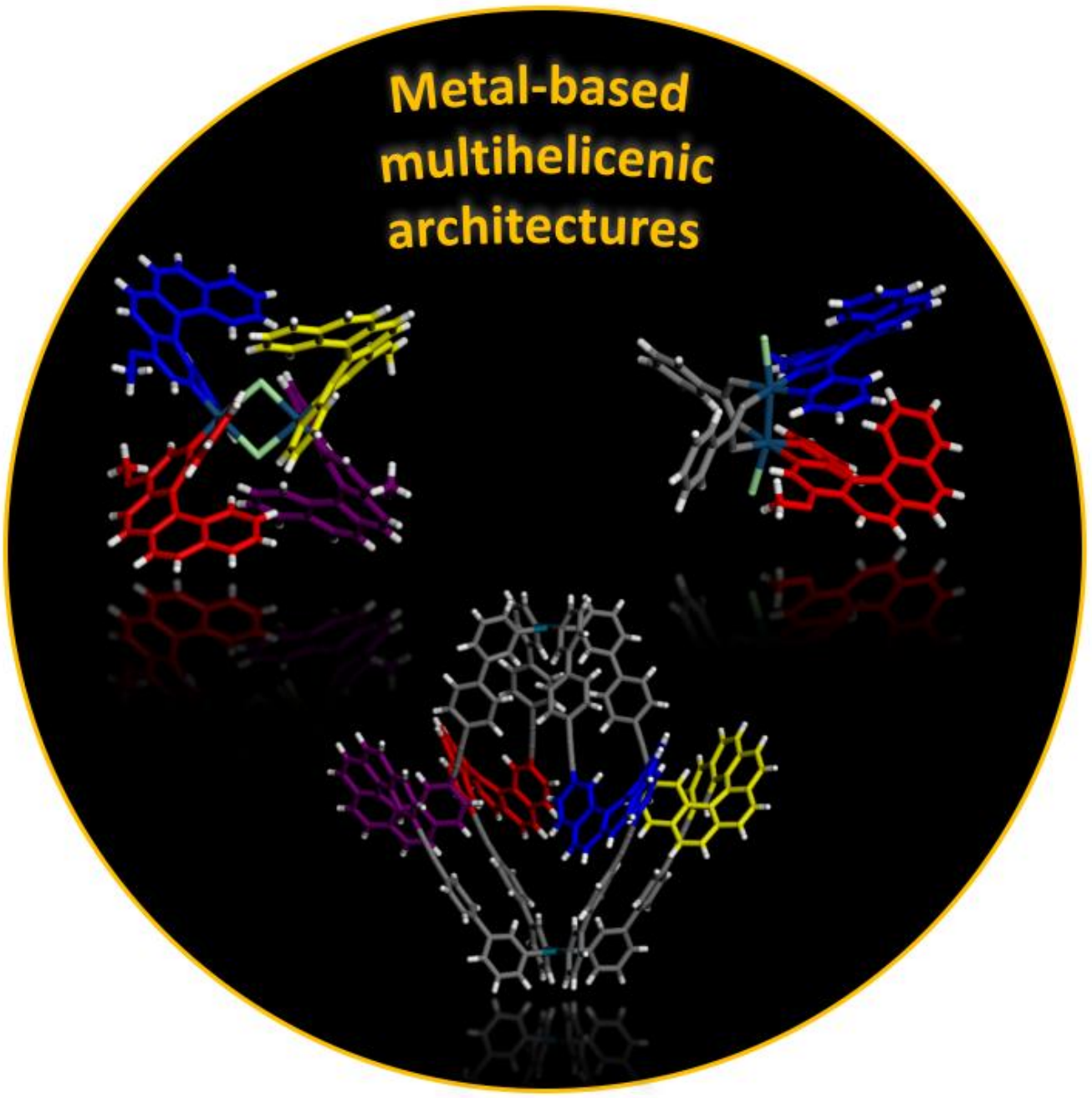

[a] Etienne S. Gauthier, Dr. Rafael Rodríguez, Dr. Jeanne Crassous
Univ Rennes, CNRS, ISCR - UMR 6226,
F-35000 Rennes, France.
E-mail: jeanne.crassous@univ-rennes1.fr

10.1002/anie.202004361

WILEY-VCH

MINIREVIEW

Abstract: The preparation of multihelicenic systems by conventional organic synthesis is a challenging task and under continuous development. In parallel, using complexing units grafted to or incorporated within the helicene core and taking advantage of coordination/organometallic chemistry constitutes a powerful strategy to obtain multihelicenic structures. This minireview focuses on the state-of-the-art preparation of metal-based multihelicenic architectures such as coordination-driven supramolecular assemblies and organometallic architectures. Their properties and their applications are presented.

1. Introduction

Helicenes are chiral polycyclic molecules formed of *ortho*-fused aromatic rings.[1] They are known to exhibit not only strong chiroptical activity (optical rotation, electronic and vibrational circular dichroism, and even circularly polarized emission) but also many other characteristics such as good conductivity, spin filtering, self-assembly, biological activity, catalytic reactivity.[1-4] They are good candidates for potential applications in materials science including non-linear optical (NLO) devices,[5] chiral wave-guides,[6] chiroptical switches,[7] molecular motors,[8] chiral OLEDs,[9] transistors,[10] or spin-based devices.[11] The chemistry of these compounds has recently grown from the stage of an academic curiosity to an important field of research, and several reviews have been dedicated to purely organic carbohelicenes or heterohelicenes.[1-4] Recently, organic multihelicenic structures have been attracting special attention and published examples are growing fast due to beautiful synthetic challenges and for materials science applications.[12,13]

While organic synthetic methods to access enantiopure compounds are well-developed, general strategies giving enantiopure coordination and organometallic complexes are also useful to construct multihelicenic architectures.[14,15] Firstly, metals are powerful templates for assembling π–conjugated ligands into well-defined molecular structures, simply by using the basic concepts of coordination and organometallic chemistry.[16] Secondly, coordination and organometallic chemistry offer simple ways to tune the optical, chiroptical and electronic properties of the π-ligands since the topology together with the nature of the metal-ligand and ligand-ligand interactions can be readily modified by varying the metal center, its associated coordination sphere geometry, its redox state, etc.[17,18] As a result, novel properties may appear when metallic ions are combined with π-helical structures and new applications may be targeted.

In this review, we describe the different types of metallo-multihelicenic architectures reported to date. Our review starts from overview of metal-based multihelicenic architectures formed by coordination assembly of monotopic or multitopic heterohelicene ligands then we describe organometallic multhelicenic systems, *i.e.* multiple helicenes bearing metal-carbon σ bonds. We discuss the chemical and configurational stabilities upon complexation, stereoselectivity and the kinetic/thermodynamic aspects upon preparation, together with the properties displayed by each class of compounds, as results of the metal used. When appropriate, we make comparison with the corresponding monohelicenic structure. The synthesis of ligands will not be discussed here, neither organic anions formed by action of a metal.[19,20] Furthermore, we focus on molecular systems; examples involving deposition of organic helicenes onto metal surfaces or nanoparticles are not presented.

Etienne S. Gauthier studied organic chemistry at the Rennes Graduate School of Chemistry (ENSCR, France) where he obtained an Engineering diploma associated with a MSc in molecular chemistry (Rennes I University) in 2017. He is currently a PhD student working under the supervision of Dr. Jeanne Crassous focusing on helicene-NHCs and the study of their synthesis, their properties and their applications notably in chiral organometallic complexes (fellowship from the ANR French National Agency).

Rafael Rodríguez received his MSc, Master and PhD at the University of Santiago de Compostela/CiQUS (Spain) working on the structural elucidation and applications of stimuli responsive helical polymers under the supervision of Prof. Félix Freire and Prof. Emilio Quiñoá. Shortly after defending his PhD, he moved as Assistant Professor to the WPI NanoLSI Institute at Kanazawa University (Japan) working on CPL active materials at Prof. Katsuhiro Maeda's laboratory. Nowadays he is a postdoctoral researcher at the Institut des Sciences Chimiques de Rennes (University of Rennes, France) under the supervision of Dr. Jeanne Crassous working on helicene-based supramolecules and polymers with CPL activity.

Jeanne Crassous (born Costante) received her Ph.D. in 1996 under the supervision of Prof. André Collet (ENS, Lyon, France), working on the absolute configuration of bromochlorofluoromethane. After a one-year postdoctoral period studying the chirality of fullerenes in Prof. François Diederich's group (ETH Zurich, Switzerland), she received in 1998 a CNRS researcher position at the ENS Lyon. In 2005 she joined the Institut des Sciences Chimiques de Rennes (University of Rennes, France). She is currently Director of Research at the CNRS. In 2013, she became a distinguished member of French Chemical Society (Société Chimique de France, SCF); in 2020, she received the national SCF Prize of the Organic Chemistry division. Her group is dealing with many fields related to chirality: organometallic and heteroatomic helicenes, fundamental aspects of chirality such as parity violation effects, chiroptical activity such as electronic and vibrational circular dichroism, or circularly polarized luminescence.

10.1002/anie.202004361

2. Coordination of mono or multidentate ligands toward multihelicenic systems

Helicene derivatives possessing N, O or P coordinating atoms and displaying either mono, bis, tris or multidentate coordination abilities, have been prepared and have been reacted with many types of metallic ions such as Ag(I), Cu(I), Zn(II), Rh(I), Pd(II), Ni(II), or Au(I), and also to multimetallic building blocks with adapted geometry. This strategy thus gave access to a great variety of coordination assemblies with different topologies and architectures, such as monometallic multihelicenic molecular systems, helicates, ladder-type polymers, supramolecular U-shaped assemblies and rectangles, infinite supramolecular columnar systems or supramolecular cages. All of them display different appealing properties among which strong optical rotations (ORs), intense electronic circular dichroism (ECD) and high circularly polarized luminescence (CPL). Many applications have been targeted, among which chiral recognition and sensing, asymmetric catalysis, chiroptical switching activity or non-linear optical (NLO) activity.

2.1.1. Monodentate azahelicenes and phosphahelicenes

The introduction of nitrogen atoms within the helical scaffold of helicenes opened the possibility of using them not only in enantioselective catalysis[21] and in optoelectronics,[22] but also as ligands in coordination chemistry. Interesting examples are the azahelicenes studied by Stara, Stary and coworkers in 2008.[23] They have successfully synthesized optically pure 1- and 2-aza[6]helicenes (**1** and **2**, respectively) and studied their assembly into supramolecular structures by coordination with Ag(I). Indeed, mixing silver(I) triflate with racemic **1** or **2** afforded the corresponding 1:2 Ag(I) pyridohelicene complexes, that were characterized by X-ray crystallography. For instance, the assembly of 1-aza[6]helicene **1** generated a homochiral [Ag(**1**)$_2$(*n*-PrOH)](OTf) complex (see **3a** in Figure 1) with T-shaped geometry where the coordination sphere of the silver atom adopts a trigonal bipyramid geometry. Thus, **1** binded the cation as an η^3-(*N*,*C*,*C*) ligand, occupying the C=C bond and N at the equatorial and axial positions. A homochiral [Ag(**2**)$_2$(OTf)](OTf) complex (**3b** in Figure 1) was formed and a T-shape coordination geometry was also observed. The preference for the coordination to silver of 1-aza[6]helicene compared to 2-aza[6]helicene was observed in the gas phase by competitive experiments, highlighting the higher basicity of the nitrogen as the driving force to promote this effect. Similar stereoselectivity toward homochiral assembly was also obtained in the gas phase. Indeed, the authors observed the formation of homochiral Ag(I) complexes with **1** in the gas phase.[24] For this, they prepared enantiopure deuterated form of 1-aza[6]helicene[7,8D$_2$] ([7,8D$_2$]-**1**), coordinated it to Ag(I) in the presence of **1** and generated homochiral complexes in the gas phase, as observed by electrospray mass spectrometry. The latter experiment demonstrated the preference in the formation of homochiral complexes (*P*,*P*/*M*,*M*) compared with the achiral one (*P*,*M*) with formulae [LAgL']$^+$ (L,L'= **1** or [7,8-D$_2$]-**1**). The distinction in the formation of homo/heterochiral assemblies of 1-aza[n]-helicenes (n= 1-7) with alkaline cations (i.e., Li$^+$, Na$^+$ and K$^+$) was also studied by Alkorta *et. al.,* by means of DFT theoretical calculations, showing to be especially remarkable in the case of lithium with n = 6 ligand.[25] Through these studies, the presence of a larger racemization barrier of the complexes compared with the uncoordinated ligands was also demonstrated.

Chiral phosphines are amongst the widest used ligands in coordination chemistry and enantioselective catalysis. Voituriez, Marinetti and coworkers recently reported the preparation of new bis-benzo-fused phospha[6]helicenes ((*P,R*$_P$*)-**4**),[26] with defined *P* chirality at the helicenic moiety and epimeric R_P/S_P configuration at the P atom. The reaction of this ligand with PdCl$_2$(MeCN)$_2$ generated the corresponding *trans*-Pd(**4**)$_2$Cl$_2$ complex with defined (*P,P*,*S*$_P$,*S*$_P$) configuration as unambiguously demonstrated by X-ray studies. This result shows that upon coordination the P atom can adapt its configuration to the helicene's one. The process is thus stereoselective (see also below on paragraph 2.2.2). Note that in the solid state columnar assemblies of molecules were observed, closely packed through edge-to-face (CH-π) interactions.

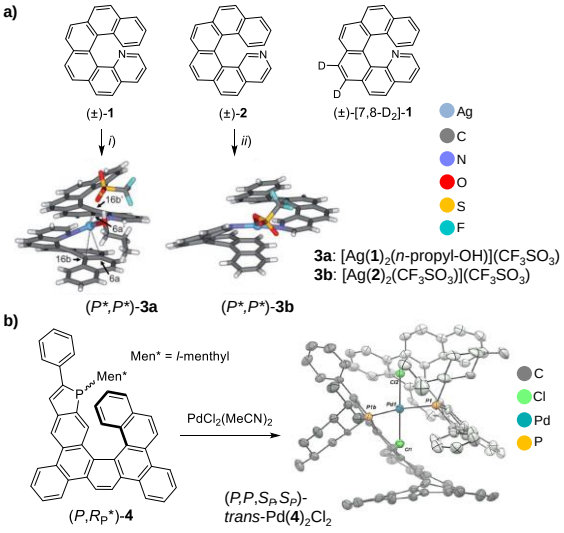

Figure 1. a) 1 and 2-Azahelicene racemic ligands (±)-**1**, (±)-**2** and (±)-[7,8-D$_2$]-**1** studied for coordination with Ag(I) and X-ray crystallographic structures of homochiral Ag^I-bis-1-aza[6]helicene complexes ((*P**,**P*)-**3a,b**). b) Phosphahelicene (*P,R*$_P$*)-**4** and its Pd(II) complex (*P,P*,*S*$_P$,*S*$_P$)-*trans*-Pd(**4**)Cl$_2$. Adapted with permission from refs. [23] and [26]. Copyrights 2008 and 2019 Wiley-VCH.

10.1002/anie.202004361

2.1.2. Monodentate cyano-capped helicene derivatives

Metal-based chiral supramolecular architectures of precise topology can be targeted by mixing chiral organic ligands with bis-metallated building blocks of known geometry. In 2014, Réau, Crassous, Lescop, and coworkers reported the preparation of dissymmetrical U-shape π-stacked supramolecular assemblies using a bis-pyridyl-phosphole, copper(I) and monotopic π-conjugated helical ligands.[27] The bis-2(2-pyridyl)-phosphole ligand **5** acted as an (*N,P,N*) tridentate ligand that —upon coordination with Cu(I)— generated pincer-like structure **6** holding a Cu(I) dimer (Figure 2a,b). The addition to this system to monotopic [4]helicene derivatives (**7a**,**b**) endowed with cyano groups (having different linkers between the CN moiety and the [4]helicene, see Figure 2b) gave rise to the formation of symmetrical U-shaped complexes **8a**,**b** shown in Figure 2c. In these complexes, the [4]helicene units display similar *M* or *P* stereochemistry in the solid state. These U-shaped complexes possess the ability to form head-to-tail supramolecular heterochiral dimers, with a large portion of the ligands being involved in π-π interactions, as depicted in Figure 2d. In their turn, the above-mentioned network of π-π interactions between the aromatic ligands inside the crystal promoted the formation of infinite columnar aggregates (see **7b** in Figure 2e). Note that in solution, *i*) such a structure probably undergoes fast exchange processes, and *ii*) the aza[4]helicene units possess overall planar geometry.

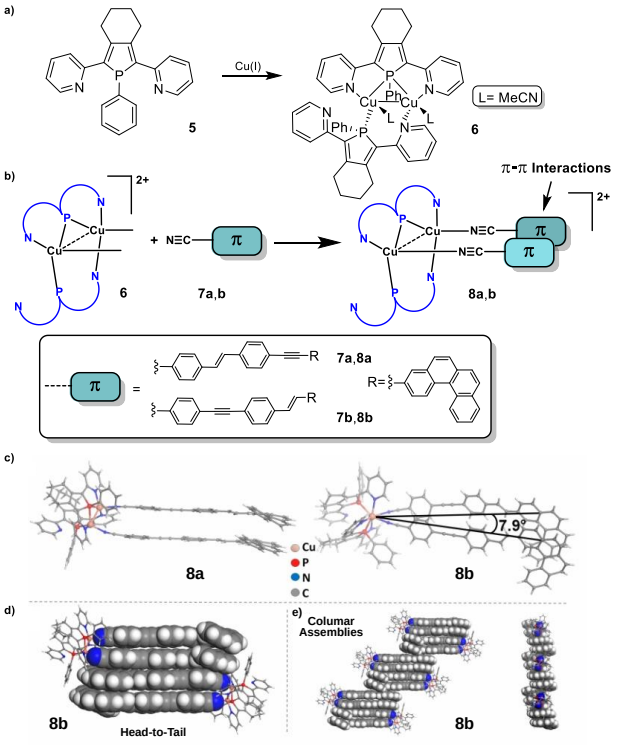

Figure 2. a), b) Chemical structures of **6**, **7a**,**b** and **8a**,**b**. c) X-ray structures of **8a**,**b**. d) Heat-to-tail supramolecular interactions and e) its infinite columnar assembly in **8b**. Adapted with permission from ref. [27]. Copyright 2014, Wiley-VCH

2.2. Bidentate helicene derivatives

2.2.1. Bishelicenic ligands for catalysis

Katz and coworkers reported the efficient multigram-scale synthesis and characterization of bis[5]helicenediol **9**, known as [5]Helol (Figure 3). The presence of two enantiopure helicenes and the well-located 2,2'-hydroxy groups generates a unique chiral pocket —that benefits from both the helicity and the axial chirality of the system— which enabled its use in asymmetric synthesis and in chiral sensing.[28] Subsequent coordination of Zn(II) to the hydroxy groups, generated an asymmetric catalyst which proved efficient in the addition of diethylzinc to benzaldehydes with enantioselectivities up to 81%. Yamaguchi and coworkers prepared phosphite **10** bearing a bis-helicenol and a chiral menthyl unit, displaying within a single molecule helical, axial and central chirality. This system was effective in the rhodium-catalyzed enantioselective hydrogenation of di-methyl itaconate with enantiomeric excess (*ee*) values up to 96%. Interestingly, the helicity of the helicene moiety played a major role in the asymmetric induction. In addition, an important match/mismatch effect in between helical and axial chirality was observed.[29] Note for comparison that the same group employed macrocycles such as **11** composed of 1,12-dimethylbenzo[c]-phenanthrene-5,8-dicarboxamides units for the addition of Et_2Zn to different benzaldehydes, obtaining moderate values in enantioselectivity (up to 50% *ee*'s).[30]

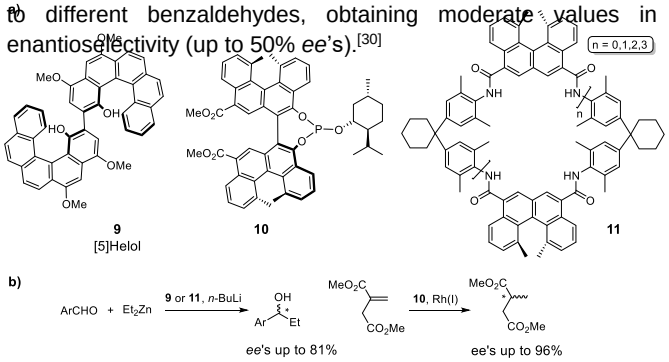

Figure 3. a) Structure of bis-helicenic systems **9**-**11** used in enantioselective catalysis. b) Enantioselective addition of diethylzinc to a benzaldehyde and enantioselective hydrogenation of di-methyl itaconate catalyzed by Rh(I).

2.2.2. Bipyridine-based helicene ligands

Thanks to their strong chiroptical responses, multihelicenic systems can be utilized as molecular chiroptical switches using either their OR, ECD, or CPL response as the read-out value and by applying a diversity of stimuli, such as light, redox potential, acids or bases, metallic ions, etc. To be efficient, the switching process should show good reversibility between at least two different states, reproducibility and good fatigability (Figure 4d).

In order to create new stimuli-responsive materials based on metal coordination, our group prepared in 2019 the bis-helicenic 2,2´-bipyridyl (bipy) system (see (*P*,*P*)-**12** in Figure 4a).[31] The presence of the central bipy system in **12** allowed the modification of the chiroptical properties upon coordination to Zn(II). The titration of **12** with $Zn(OAc)_2{\cdot}2H_2O$ produced a conformational motion within the bridging bond of the bis-helicenic system, which changed from a *trans* to a *cis* arrangement, thus behaving as a molecular hinge (Figure 4b) that was traduced into a concomitant variation in the ECD and UV-vis spectra until saturation of the coordinating moiety (1.0 eq Zn(II), Figure 4c). Note that the presence of two helicene units in the system gives very strong

ECD responses ($\Delta\varepsilon$ values up to 400 M^{-1} cm^{-1}). Furthermore, the fluorescence and CPL responses underwent a red shift upon metal coordination. Indeed, the CPL responses measured in CH_2Cl_2 at rt showed maximum g_{lum} values ($2\Delta I/I$) of $+4.8 \times 10^{-3}$ for (*P*,*P*)-**12** at 425 nm, and $+1.8 \times 10^{-3}$ for (*P*,*P*)-**12**·$Zn(OAc)_2$ at 495 nm. This process appeared fully reversible upon addition of *N*,*N*,*N*´,*N*´-tetrakis(2-pyridylmethyl)ethane-1,2-diamine (TPEN) as metal scavenger which regenerated the initial chiroptical properties of (*P*,*P*)-**12**. Furthermore, using triflic acid, protonation of the nitrogen atoms of the pyridyl rings within the helicenic structure was performed and the fluorescence and CPL spectra displayed a strong red shift (>150 nm). Indeed, the CPL responses of (*P*,*P*)-**12**·$2H^+$,$2OTf^-$ measured in CH_2Cl_2 at rt (see Figure 4c) showed a distinct signal centered around 605 nm with a g_{lum} factor of $+2.5 \times 10^{-3}$ for the (*P*,*P*) enantiomer, *i.e.* of the same order of magnitude as those found for **12** and **12**·$Zn(OAc)_2$ but much more red-shifted. This process appeared reversible since deprotonation using addition of Et_3N regenerated (*P*,*P*)-**11**. This system therefore represents an interesting example of fully reversible CPL switch between three different states activated with different chemical stimuli.

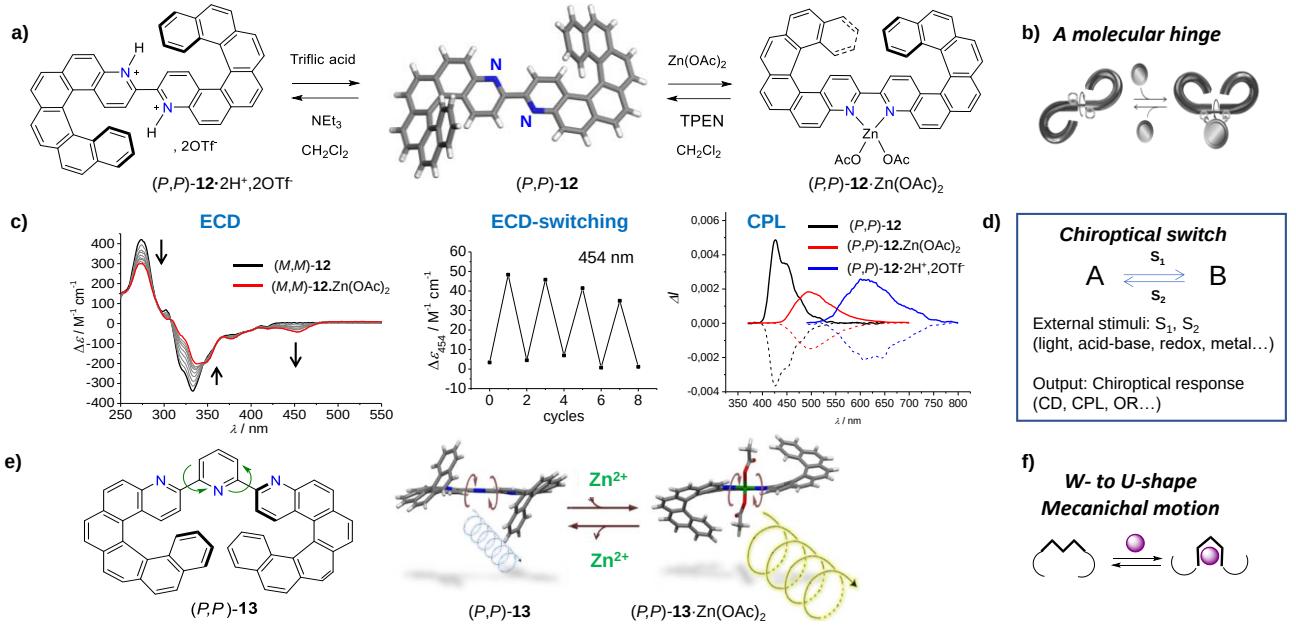

Figure 4. a) Molecular structures of (*P*,*P*)-**12** ligand, (*P*,*P*)-**12**·$Zn(OAc)_2$ complex and of (*P*,*P*)-**12**·$2H^+$,$2OTf^-$. b) Sketch of a molecular hinge. c) Switching process between initial and final states throughout the titration with $Zn(OAc)_2$·$2H_2O$ followed by ECD switching process at 454 nm. CPL spectra of (*P*,*P*)/(*M*,*M*)-**12**, (*P*,*P*)/(*M*,*M*)-**12**·$Zn(OAc)_2$ and (*P*,*P*)/(*M*,*M*)-**12**·$2H^+$,$2OTf^-$. d) General sketch of a chiroptical switch. e) Chemical structure of bis-helicenic terpy ligand (*P*,*P*)-**13** and its reversible reaction with Zn^{2+} provoking the CPL-tuning together with reverse process. f) Sketch of W- to U-shape conformational change. Adapted with permission from refs [31] and [38] Copyrights 2019, ACS and 2016, RSC.

2.2.2. Assembly of heteroditopic azahelicene-phosphole ligands

The incorporation of two distinct atoms with different coordinating properties (i.e., a soft P and a hard N donor) enclosed within the same ligand framework is an interesting way to increase the structural complexity of the supramolecular assemblies thus generated. In this regard, our group prepared such kind of heteroditopic ligands based on phospha-azahelicenes possessing a 1,4-chelating moiety for transition metals. The first work was reported by Crassous, Réau *et. al.*[32] through the preparation of (*P*,*N*) ligands bearing a short [4]-azahelicene, such as **14** in Figure 5. The coordination of such ligand with Pd(II) or Cu(I) —presenting square planar and tetrahedral coordinating geometry, respectively— gave rise to metallo-organic bis-helicenic assemblies with different 3D-structures. Indeed, the assembly of **14** with $[Pd(MeCN)_4(SbF_6)]$ in dichloromethane generated in a stereoselective way the complex **15** of formula $[Pd(\mathbf{14})_2](SbF_6)_2$ as demonstrated by NMR and X-Ray studies (Figure 5a). The *trans* effect was the driving force for the stereoselective formation of this family of complexes displaying C_2 symmetry and parallel arrangement of the two (*P*,*N*) chelates. The coordination with a tetrahedral cation was then tested, through the assembly of **14** with $Cu(MeCN)_4BF_4$ in CH_2Cl_2, which generated complex **16** of formula $[Cu(\mathbf{14})_2](BF_4)$ with distorted tetrahedral geometry, in which the two azahelicenes are in almost in a perpendicular arrangement around the Cu(I) cation (Figure 5a). The two stereogenic elements, *i.e.* the [4]helicene and the P atom, interconvert rapidly at room temperature due to their low inversion barrier ($\Delta G^{\#}$ = 16.4 kcal.mol^{-1} for the phosphole),[33] and the Pd(II) or Cu(I) coordination processes appeared highly stereoselective, as shown by X-ray crystallographic structures of assemblies **15** and **16** in the solid state and by NMR spectroscopy in solution. Indeed, among all the possible stereoisomers that could be formed, only the C_2-symmetrical Pd(II)–bis(helicene) **15** was observed in the crystal as a couple of enantiomers, *i.e.* [(*M*,*M*,S_P,S_P,Λ_{Pd}) and (*P*,*P*,R_P,R_P,Δ_{Pd})]. Similarly, the copper-based (*P*,*M*,S_P,S_P,Λ_{Cu}) and (*M*,*P*,R_P,R_P,Δ_{Cu}) assemblies were obtained for **16**. The high fidelity on the stereoselectivity through the coordination process was also unambiguously demonstrated in solution through the ^{31}P and ^{1}H NMR spectra obtained.

10.1002/anie.202004361

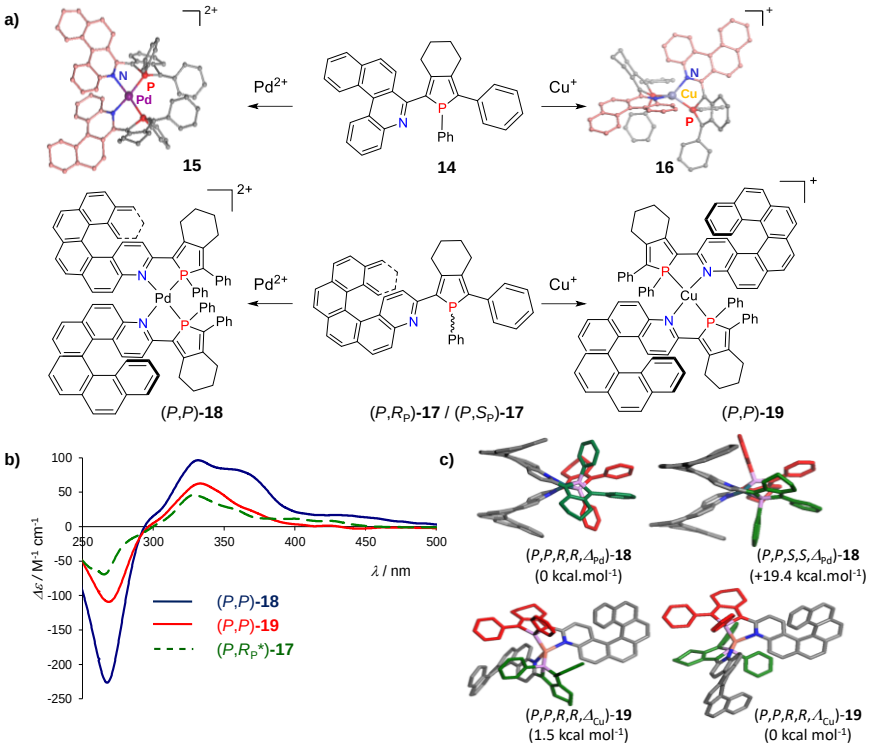

Figure 5. a) Structures of ligands **14** and **17** and of the assemblies generated with Pd(II) and Cu(I). b) ECD spectra of ligand (*P*,R_P*)-**17** and of complexes (*P*,*P*)-**18** and **19** showing the presence and absence of active MLCT bands for the Pd and Cu complexes respectively. Calculated structures of c) Pd(II) complex **18** showing a great energetic difference between both diastereomers and d) of Cu(I) complex **19** showing small energetic differences between both diastereomers. Adapted with permission from refs [32] and [34]. Copyrights 2008, RSC and 2009, ACS.

Encouraged by these seminal results, our group prepared a variety of ditopic phosphol-azahelicene ligands with increasing degree of structural complexity, leading to new intriguing architectures after coordination with metal cations. Indeed, Crassous, Réau and coworkers reported the preparation of phosphole **17** substituted with an enantiopure configurationally stable 2-aza[6]helicene and its incorporation into supramolecular structures generated by metal coordination (Figure 5a).[34,35] An epimeric (*P*,R_P*) mixture was obtained due to the easy inversion of the P atom. Subsequent complexation to Pd(II) and Cu(I) generated bis(helicene) complexes **18** and **19**. Interestingly, Pd(II) showed higher efficiency than Cu(I) to organize two aza[6]helicene-phosphole ligands around the metallic ion in a highly stereoselective way. The combination of steric hindrance, *trans* effects and the configurational lability at the P atom of the phosphole creates a unique scenario for the generation of such complexes. Thus, the P atom is able to adapt its stereochemistry to minimize the congestion between the two ligands **17** and the alignment in a *cis* orientation of the two (*P*,*N*) chelates around the Pd(II) atom. The *P* handedness of the [6]helicene controls the *R* configuration in the P atom, finally inducing *Δ* configuration on the Pd atom. Structural insights were successfully obtained by means of DFT calculations, demonstrating the (*P*,*P*,R_P,R_P,Δ_{Pd})-**18** diastereomer to be 19.4 kcal mol^{-1} more stable than the (*P*,*P*,S_P,S_P,Δ_{Pd})-**18** one. Interestingly, analogous studies on the Cu(I) complex **19** revealed that several diastereoisomers present similar energies, therefore the coordination around the tetrahedral Cu(I) is not stereoselective (Figure 5c). The exquisite stereoselective Pd(II) assembling process promoted the enhancement of the chiroptical properties compared with the ligand or the analogous Cu(I) assembly. ECD spectrum of the (*P*,S_P)-**17** ligand displays the classical pattern for a π-conjugated helical system, with π–π* being the main electronic transitions along the helicene-phosphole unit (Figure 5b). In the palladium complex (*P*,*P*)-**18**, the presence of ECD active bands around λ = 400-500 nm indicate the successful chiral induction from the helicene to the metal-ligand electronic interactions in the MLCT transitions. On the contrary, the Cu(I) complex (*P*,*P*)-**19** does not exhibit low energy bands in the ECD region, a point that is directly related with the low stereoselectivity observed during the assembly process.

2.2.3. Coordination cages based on helicenes

Recently, Clever and coworkers reported the assembly of different pyridine-based helicenes with $[Pd(CH_3CN)_4(BF_4)_2]$ as a source of square-planar palladium cations generating quadruple-stranded Pd_2L_4 cages (Figure 6).[36] They initially designed two different systems where the central helicene moiety was endowed with either a bis(3-pyridylethynyl) (**20**) or a bis(3-(pyridylethynyl)phenyl) (**21**) unit, thus resulting in ligands with a different length between the helical core and the coordinating unit (Figure 6a). Firstly, they compared the assembly of a racemic mixture *vs.* the enantiopure version of **20**. Interestingly, the racemic mixture generated in a quantitative way a *meso* Pd_2L_4 complex **C1**^{meso} —under a chiral self-sorting process— involving two *P* and two *M* ligands. The assembly of the enantiopure form,

i.e. either *P* or *M* ligand **20** under the same conditions generated the homochiral Pd_2L_4 **C1**$^{P/M}$. The structures of both enantiopure and racemic complexes were unambiguously confirmed by ^{1}H NMR, HRMS and X-ray techniques.

With the aforementioned Pd_2L_4 in hands, the host-guest properties of these capsules were studied. As target guests, *R*- or *S*-camphorsulfonate **G1** anions were tested. Unfortunately, both enantiopure and meso cage did not lead to any host-guest complex formation, most likely due to the limited size of the cage inner space (Figure 6b). In order to increase the inner volume of the capsule and increase the chances of having a capsule with enantio-discriminating properties authors turned their attention into the cage generated by **21**, where the introduction of the 1,4-phenylene moiety led to a two-fold increase of the Pd-Pd distance as demonstrated by DFT calculations. Following the same protocol as for **20**, ligand **21** was assembled with Pd cations into Pd_2L_4 cages **C2**$^{P/M}$ in both racemic and enantiopure versions. The racemic ligand gave rise to a statistical mixture of isomeric species as supported by the appearance of several sets of peaks in ^{1}H NMR and only peaks assignable to the tetracationic species in mass spectrometry and superimposable with the enantiopure version. The lack of self-discrimination in the formation of the cages was explained by the increased size of the ligand, giving rise to lower interaction between the helical backbones of the helicene-based ligands. Interestingly, when the self-assembly process was carried out in MeCN instead of DMSO a totally different scenario was observed. Under this condition, the interpenetration of two M_2L_4 capsules **C2**$^{P/M}$ took place generating the dimeric interpenetrated M_4L_8 complex **DC2**$^{P/M}$ (Figure 6c) as demonstrated in solution by the splitted NMR resonances and the presence of the corresponding signals of the dimeric capsule in MS spectrometry. The structure was unambiguously assigned by X-ray crystallography, showing twelve ligands inter-twinned in a remarkable ordered fashion. Additionally, the dimeric cage presents three consecutive pockets, with the two outer ones occupied by one PF_6^- anion from the crystallization process.

The presence of a larger void volume gave rise to selective guest encapsulation of **G1** within the chiral walls of the cage. Indeed, ^{1}H NMR titrations of **G1**^{R} and **G1**^{S} as tetrabutylammonium salts with either *P* or *M*-based capsule showed a stronger extent for the diastereomeric encapsulation (**G1**^{R}**@C2**^{P}/**G1**^{S}**@C2**^{M}) compared with the enatiomeric one (**G1**^{S}**@C2**^{P}/**G1**^{R}**@C2**^{M}) with binding constants of 1010 M^{-1} and 560 M^{-1}, respectively (Figure 6d). Additionally, these capsules are able to discriminate between anionic guests with different geometries yet similar structure, *i.e.* 2,7-naphtalenedisulfonate **G2**, 4,4´-biphenyldisulfonate **G3** (short and long guest respectively) and an azobenzene disulfonate **G4** in *cis*- and *trans*- geometry. The encapsulation of these different species, even though being achiral, led to a variation in the ECD spectra of the generated species (Figure 6e). This effect is directly related to the variation of the pitch of the helicenic backbone, where longer helical pitches produce an increase in the ECD spectra. Additionally, this compressing/stretching process of the capsule triggered by the host-guest complex formation was also demonstrated by ion mobility ESI-TOF mass spectrometry (TIMS TOF) (Figure 6f).

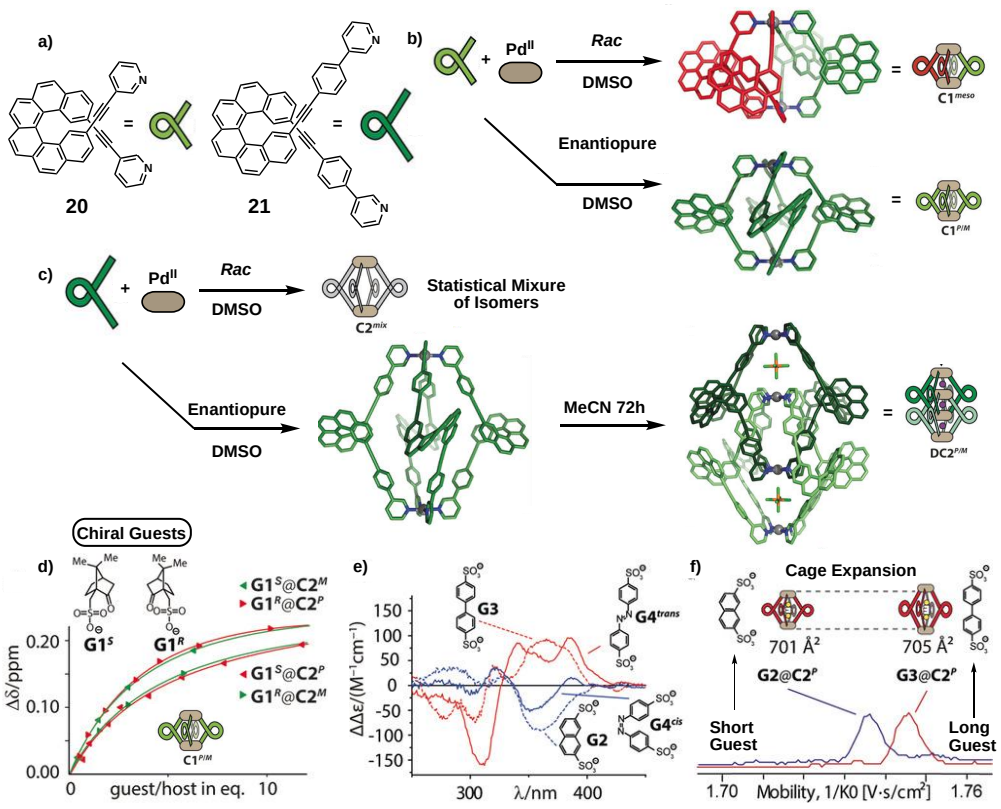

Figure 6. a) Structure of **20** and **21**. Schematic illustration of the corresponding capsules generated by self-assembly with square-planar Pd cations with b) **20** and c) **21**. d) ^{1}H NMR titration of **G1**/**G2** onto capsule **C2** depicting enantioselective encapsulation. Cage expansion/contraction process of **C2** through encapsulation of large/short guests of **G2**-**G4** supported by e) ECD and f) ion mobility experiments. Adapted with permission from ref. [36]. Copyright 2019, Wiley-VCH.

10.1002/anie.202004361

2.3. Tridentate helicenic derivatives

2.3.1 Terpyridine-based bishelicenic ligand

Inspired by the seminal report of Lehn and coworkers in the conformational control by metal coordination from W to U shape of terpyridine units,[37] our group reported the preparation of enantiopure terpyridine-based bis-helicenic system **13** whose conformation and chiroptical properties can be modulated upon addition a chemical stimulus (see Figure 4c).[38] The addition of increasing amounts of a proper transition metal source (i.e., Zn(II)) resulted in the formation of (*M,M*)- and (*P,P*)-**13**·Zn(OAc)$_2$ and produced a significant variation of the ECD, UV-Vis spectra. Theoretical calculations showed that the low-energy bands corresponded to a charge-transfer type transition while in the starting ligand ECD was mainly assigned as π–π* transitions. The spectroscopic changes in the ground state were also accompanied by changes in the excited state. Indeed, upon metal coordination, the vibronically-structured fluorescence at 419 nm of the ligand (*P,P*)-**13** displaying a g_{lum} value of $+6.8 \times 10^{-3}$ shifted towards a structureless intense fluorescent band centered at 480 nm with a g_{lum} value of 1.1×10^{-3} for the (*P,P*)-**13**·Zn(OAc)$_2$ complex. Interestingly, this process was fully reversible upon addition of TPEN as a metal scavenger (chiroptical switching process). Therefore, the chiroptical properties of this system could be efficiently modified by taking advantage of metal coordination switching the architecture of the system from U to W shape (Figure 4f), thus inducing a strong conformational change.

2.3.1 Coordination of bis-azahelicene-phosphole

In relation to the above mentioned results on tritopic (*N,P,N*) bipyridyl phosphole (see 2.1.2) and ditopic (*P,N*) phosphole-azahelicene assemblies (2.2.2) was reported the preparation of a new bis(aza[4]helicene)-phosphole **22** (Figure 7).[39] This new ligand possesses a tridentate (*N,P,N*)-pincer structure suitable for assembling it into more complex architectures after metal coordination. The assembly of ligand **22** with Cu(I) cations in the presence of two dicyano-stilbene **24** and two dppe ligands generated a unique tetrametallic tetrahelicenic supramolecular assembly **25** with rectangular shape that resembles the structures of paracyclophanes. During the process, a highly efficient self-assembly took place generating a bimetallic building block **26** where the bis-helicenic (*N,P,N*)-pincer coordinates to two Cu(I) atoms —with the P atom of the phosphole ring behaving as a bridging μ-P-donor— that are also connected through the dppe ligand and display a cuprophilic interaction (see X-ray structure in Figure 7c). Interestingly, the cyano-stilbene molecules acted as bridges connecting two pincer building blocks **23** generating the rectangle-like supramolecular structure **25** (see chemical structure in Figure 7b and X-ray in Figure 7c). Single crystal X-ray diffraction of **25** revealed the presence of π-π interactions between the two bridging cyano-stilbene of the rectangle, these interactions being the driving force for the generation of the supramolecular assembly. Note however that in solution, *i*) such a structure probably undergoes fast exchange processes, and *ii*) the aza[4]helicene units possess overall planar geometry.

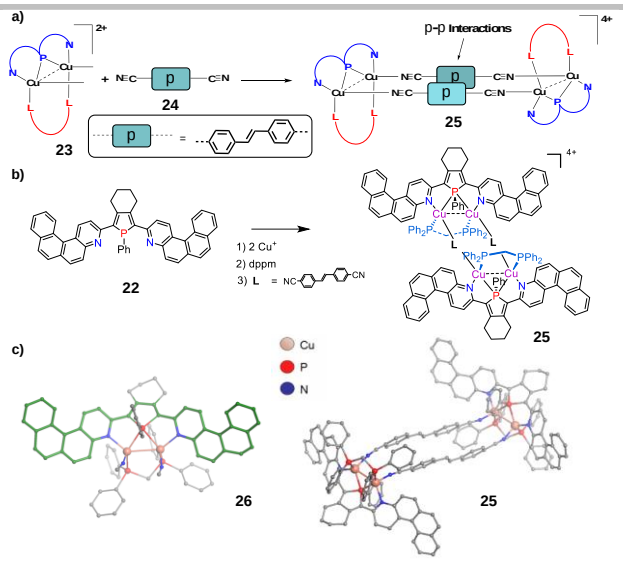

Figure 7. a) Sketch of the coordination-driven self-assembly to rectangle **25**. b) Chemical structures of (*N,P,N*) ligand **22**, and of supramolecular rectangle **25**. c) X-ray structures of bimetallic bishelicenic complex **26** and of supramolecular metallo-rectangle **25**. Adapted with permission from ref. [39]. Copyright 2011, Wiley-VCH.

2.4. Coordination of multitopic helicenic ligands

2.4.1. Multitopic azahelicene-phosphole ligands

With the idea of increasing the complexity on this kind of supramolecular assemblies, Autschbach, Crassous, Lescop, Réau *et. al*. reported in 2013 the preparation of multitopic 2,6-bis(aza[6]helicenephosphole)-pyridine (**27**) displaying a unique combination of (*N,P,N,P,N*) donor atoms (Figure 8).[40] This ligand is well-structured to generate double stranded helicates in the presence of Cu(I). The existence of enantiopure *M* or *P* helicenes allowed the preparation of enantiopure helical ligands —named helicands— that generated double-stranded helicene-capped tetrametallic helicates upon coordination with Cu(I). These helicates bear two pairs of Cu(I) dimers —displaying cuprophilic interactions, as already seen in **6**, **8a**,**b** and in **25**, **26**— coordinated to the N atoms of both aza[6]helicene and pyridine connecting unit and bridged by the P atom of the phosphole.

The helicate structure was confirmed by X-ray crystallography of 2-pyridyl and [4]helicenic based models. Furthermore, the efficient chiral induction from the azahelicene moieties towards the Cu(I) environement was unambiguously demonstrated by theoretical calculations combined with experimental results which indicated the effective chiral communication from aza[6]helicene moieties to the Cu(I) helicate core, together with the presence of helicand-to-helicand charge transfer (LLCT type) transitions that drastically impacted the ECD active bands.

10.1002/anie.202004361

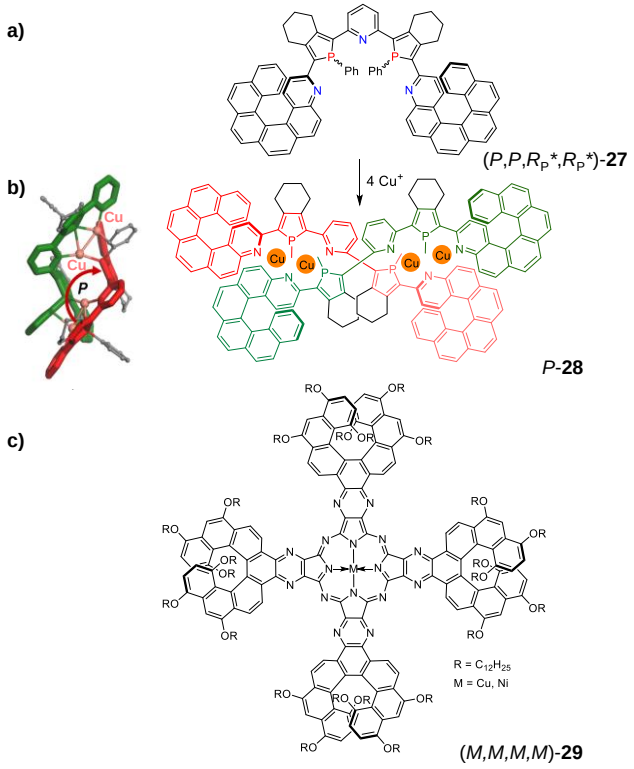

Figure 8. a) Structure of helicand (*P*,*P*,R_P^*,R_P^*)-**27** and the corresponding double-stranded helicate *P*-**28** assembled with Cu(I)-Cu(I) units. Helicand units are highlighted in red/green for clarity. b) Highlighted coordination around the Cu(I)-Cu(I) scaffold in **28**. c) Phtalocyanine **29** capped with [7]helicene and displaying strong NLO activity.

2.4.2. Multihelicenic phtalocyanine derivatives

In 1999, Katz and coworkers reported the preparation of phtalocyanines such as **29** depicted in Figure 8c bearing four [7]helicene moieties in their periphery and endowed with either Ni or Cu in the inner cavity of the macrocycle.[41] Interestingly, these molecules self-assemble into columnar stacks when dissolved in EtOH/$CHCl_3$ (75/25) and also as pristine materials. This assembly mode is also favored by the presence of each substituted with four long alkyl chains which enable van der Waals interactions. Theoretical calculations revealed that the molecules stacked with their cores separated by ca. 3.4 Å, and formed chiral superstructures. Additionally, upon deposition onto a mica surface, isolated stacks of the phthalocyanines in which the axes of stacking are perpendicular to the substrate could be observed by Atomic Force Microscopy (AFM). Thanks to the presence of the four helicene units and despite the fact of being highly symmetrical, the molecules displayed second-order nonlinear optical response when assembled in Langmuir−Blodgett films adsorbed onto a glass substrate.

2.4.3. Ladder polymers

In 1996, Katz *et al.* described the preparation of ladder copolymers **31** based on helicenes. They reported the synthesis of ligand **30** —a [6]helicene endowed with two salicylaldehyde units— and the subsequent condensation with 1,2-phenylenediamine in the presence of $Ni(OAc)_2$ (Figure 9a).[42] The obtained polymer connected through Ni-salophen units present an average molecular weight (Mn) of 7000/7400 g·mol^{-1} according to ^{1}H NMR and Gel Permeation Chromatography (GPC) measurements, respectively, *i.e.* corresponding to an octamer. Interestingly, molecular modelling of the polymer showed the presence of a helical orientation of the salophen groups along the axis of the ladder polymer (Figure 9b). This fact promotes the appearance of a strong ECD spectrum in the MLCT bands of the Ni-salophen group (Figure 9c). Following this work, the same authors succeeded in the preparation and chiroptical characterization of model complexes as well as the corresponding Cu/Co-salophen ladder polymers, presenting similar chiroptical properties in the corresponding MLCT bands on the Cu/Co salophen area.[43]

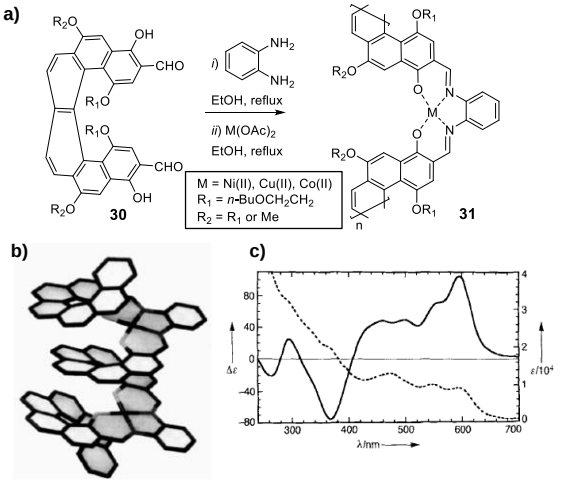

Figure 9. a) Synthetic scheme for salophen-based ladder polymer **31**. b) Calculated structure for ladder polymer **31**. c) ECD/UV-vis spectra of **31**. Adapted with permission from ref. [42]. Copyright 1996, Wiley-VCH.

3. Organometallic multihelicenic architectures

There exist different types of organometallic complexes bearing M-C bonds. The metal can be connected to a Cp ligand in a η^5-mode, a phenyl through η^2-modes, an alkynyl through a μ-type link, or a phenyl-pyridyl (*C*,*N*) ligand, through a formally (L,X)-type coordination. Many metallic ions can be used, such as Fe(II), Ru(II), Pt(II), Ir(III), Co(III), Au(I), or Ag(I). By these ways, complexes displaying redox activity, conductive properties, circularly polarized emission, and chiroptical switching activity can be targeted.

3.1. Multihelicenic metallocene derivatives

3.1.1. Cyclopentadienyl multihelicenic complexes

Cyclopentadienyl (Cp) anions are amongst the most common anionic ligands in metal complexes and are found in various organometallic compounds. Historically, in the 70-90's, pioneering work was performed by Katz and collaborators who prepared many classes of metallohelicenes from cyclopentadienyles. In 1986, they studied the preparation of enantiopure helicene-based metallocene oligomers from enantiopure bis-η^5-[9]helicenic ligand **32** (Figure 10a).[44,45] Such chiral oligomeric metallocenes were prepared with the aim of

studying potentially unusual conductivity, magnetic and (chir)optical properties. The short enantiopure oligomeric colbatocenium complex containing 2 to 4 helicenic units and linked by Co^{III} atoms was first prepared in 1986 from bis-indenyl[9]helicene *M*-(-)-**32**. Its molecular weight was identified by fast atom bombardment mass spectrometry and elemental analyses. In 1993, cobaltocenium oligomers such as **33a** were more extensively studied. Oligomers of different lengths could be obtained depending on the solvent with the longest heptameric systems obtained in toluene thanks to higher solubility. These compounds also exhibited strong chiroptical responses, with specific rotations reaching 32000-34000 and strong ECD active bands with $\Delta\varepsilon$ values between 300-1200 M^{-1} cm^{-1}.[45] However, these values corresponded to no more than the addition of several cobaltocenium units, which suggested that no efficient electronic interaction occurred between each unit (not a mixed-valence system). This was further confirmed by the cyclic voltammetry which displayed a large Co^{III}/Co^{II} reduction wave at a potential similar to the corresponding mononuclear (**34a**) and dinuclear (**35a**) species. The helical optically active bis-cobaltocenium salt **35a** was also prepared and its X-ray structure showed that the metals are far away and separated by 8.49 Å (Figure 10b). Furthermore, the difference between two Co(III)/Co(II) reduction potentials of **35a**, 130 mV, is shown to be appropriate for a conjugated dimetallocene with metals so distant. The electrochemical or chemical Co(III)/Co(II) reduction produced species that absorb near 920 nm.[46] Due to strong similarity with analogue complex bearing only one cobalt (**34a**), this absorption was not analyzed as an intervalence transition but originating from isolated Co(II) centers. The optical and electron spin resonance (ESR) spectra revealed that the unpaired electron in monoreduced form of **35a** is largely localized on cobalt and that the di-reduced form is essentially a Co(II)Co(II) diradical. Interestingly, the electrolytic reduction of cobaltocenium oligomers **33a** in acetonitrile on a Pt electrode yielded the formation of a film which appeared conductive. This film could be reversibly oxidized and redissolved. Another interesting aspect is the reversible reduction and oxidation of these oligomers in solution using cobaltocene in excess and air respectively. Significant changes were observed in the ECD spectrum of *P*-(+)-**33a** which interconverts between the fully oxidized and the fully reduced species with the presence of several isosbestic points (Figure 10c). In fact, these helical cobaltocenium oligomers synthesized were not only the first optically active polymetallocenes, but also the first polymeric metallocenes whose metals are linked by conjugated aromatic ligands. On top of that, they displayed unprecedented chiroptical switching activity. Note that isoelectronic ferrous complex (+)-**33b** was also prepared and showed huge specific rotation (± 27000), but it was impossible to obtain it in chemically pure form.[45]

The reactivity of η^5-[n]helicenic ligands as a function of n was also studied by Katz's group. In 1978, they showed that achiral bis-cobaltocenium-type (**36**) and bis-ferrocene-type (**37**) closed structures were formed instead of oligomers when using respectively short [4]helicene or [5]helicene ligands (Figure 11a).[47] Longer racemic [7]helicene ligand possessed the appropriate size to place the two cyclopentadienyl rings in front of each other thanks to a full turn of the helix leading to the formation of closed chiral structures **38a,b**.[48,49] Organometallic bis-pentahelicene ferrocene-type complex **39** was prepared by Thiel *et al.* from dibenzo[c,g]fluorenide (Dbf^-) acting as a cyclopentadienide ligand placed at a central position (Figure 11a).[50] However, **39** could not be resolved into pure enantiomers since easy racemization occurred at room temperature in solution. The reactivity of such complex upon reduction was examined. Reaction of $[(Dbf)_2Fe]$ **39** with dihydrogen and Pd/C led to the selective hydrogenation of the C3=C4 and C3'=C4' double bonds to give the corresponding 3,4,3',4'-tetrahydrodibenzo[c,g]fluorenide complexes $[(H4\text{-}Dbf)_2Fe]$ (**39'**). Configurationally stable analogues were recently prepared by Nozaki *et al.* from racemic and enantiopure 9H-cyclopenta[1,2-*c*:4,3-*c*']diphenanthrene proligand which possess a rigid helical shape formed of seven fused rings (Figure 11a).[51] While Fe(II) complexes apperead not chemically stable, bis-η^5-[7]helicenic Ru(II) complexes (**40**) could be obtained. When the racemic proligand was used, a mixture of (*M*,*M*)- and (*P*,*P*)-**40** (*rac*-**40**) was obtained together with the *meso* compound (*meso*-**40**) in a 7:3 ratio. Enantiopure bis[7]helicenic ruthenium(II) complexes were obtained from enantiopure proligands. The X-ray structure of *rac*-**40** ascertained the presence of Cp anions and their η^5-type coordination to Ru, together with lower helicity of the helical ligands compared to the fluorenyl starting material. The kinetic and thermodynamic data were estimated experimentally from the isomerization rates and the equilibrium constants at various temperatures. The activation energy of isomerization from *rac*-**40** to *meso*-**40** was found to be $\Delta G^{\neq}$ = 33.9 kcal.mol^{-1} at 400 K. It was also observed that this epimerization process underwent through inversion of the helical ligand within the complex. Interestingly, contrary to cobaltocenium helical complexes **34a**, theoretical calculations revealed that complex **40** behaved as one expanded system in which the two helical ligands are conjugated through the central ruthenium atom. Indeed, DFT calculations showed that the frontier molecular orbitals (FMOs) of *rac*-**40** are delocalized over the entire molecule and the HOMO–LUMO gap (3.27 eV) is narrower than that of the corresponding monohelicenic monoruthenium complex **40'** (see Figure 11b). This result nicely highlights the better choice of ruthenium over cobalt to obtain efficient electronic communication between the metal and he helicenic ligand (see also paragraph 3.2.2). These results were also supported experimentally by UV-vis and ECD which showed more red-shifted spectra and from specific optical rotations, which display higher values for bishelicenic (*P*,*P*)-**40** ($+2.9 \times 10^3$) as compared to monohelicenic counterpart *P*-**40'** ($+0.96 \times 10^3$). Note also that a larger contribution of the metal *d*-orbitals to the FMOs was found for **40** as compared to complex **40'** (see Figure 11b).

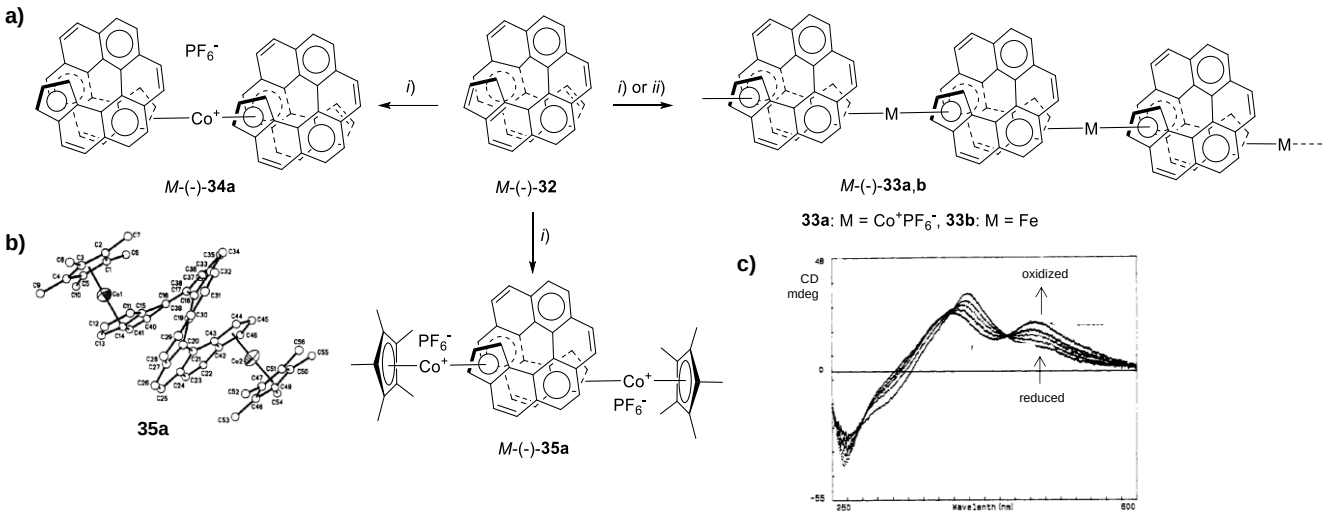

Figure 10. a) First example of oligomeric organometallic Co(III) and Fe(II) complexes *M*-(-)-**33a**,**b** and dimer complex **34a** bearing bis-η^5-helicenic ligands. *i*) 2 eq. *t*-BuLi, then $CoBr_2$.DME, oxidation with $FeCl_3$ then NH_4PF_6; *ii*) *t*-BuLi, $FeCl_2$. b) X-ray structure of helical bis-cobaltocenium salt **35a**. Adapted with permission from ref. [46]. Copyright 1993, ACS. c) Modification of the ECD spectrum of *P*-(+)-**33a** upon reduction and oxidation. Adapted with permission from ref. [45]. Copyright 1993, ACS.

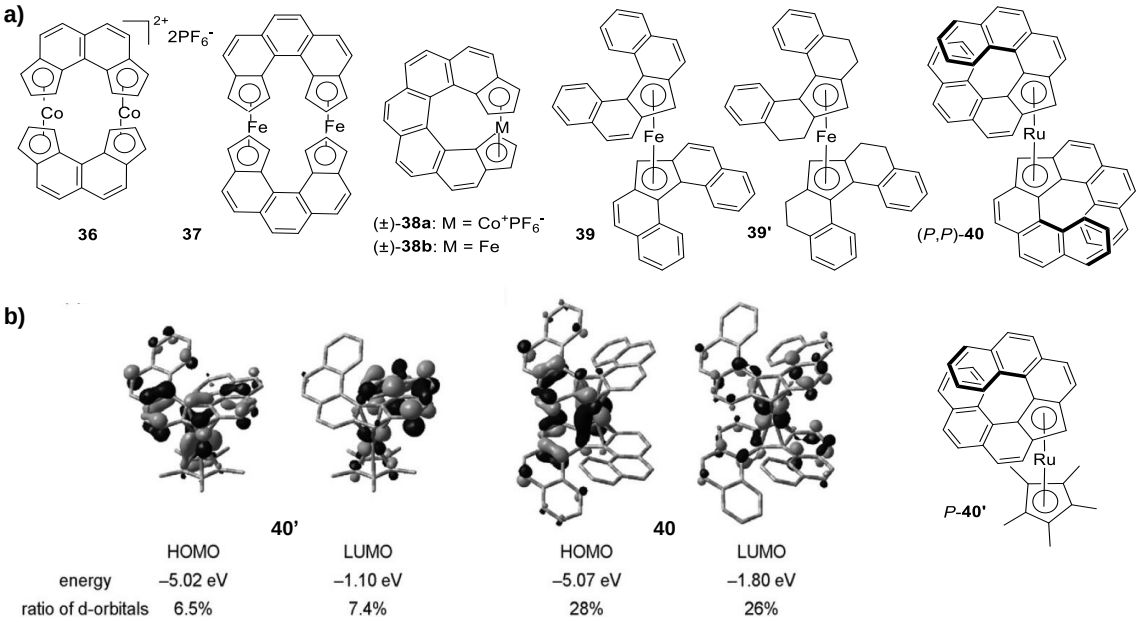

Figure 11. a) Different examples of organometallic Fe(II), Co(III) and Ru(II) complexes bearing η^5-helicenic ligands. b) HOMOs and LUMOs of *rac*-**40** and *rac*-**40'** estimated by DFT calculations. Reproduced with permission from ref. [51]. Copyright 2017, Wiley-VCH.

3.1.2. Trishelicenic phenyl-based sandwich-type complexes

Recently, Gingras, Coquerel and coworkers reported the synthesis of C_2 and D_3-symmetrical molecules **41** and **42**, respectively, possessing a triphenylene core and embedding three [5]helicene units on their inner edges and three [7]helicene units at their periphery.[52] [7]Helicene itself was earlier demonstrated to behave as a chiral molecular tweezer for silver(I) ions, the metallic cation being sandwiched between the two outermost bonds of the helicene (C_3–C_4)[53] It was then hypothesized that hextuple helicene D_3-**42** embedding three identical and moderately stretched [7]helicene units on its outer shell could behave as a mono, bis, or triple tweezer capable of complexing up to three silver(I) ions to form some original chiral cationic metal-multihelicene hybrids (Figure 12). Experimentally,

10.1002/anie.202004361

a two-step analysis (ion mobility separation IMS followed by electrospray ionization mass spectrometry ESIMS) of a mixture D_3-**42** and $AgNO_3$ (in 1:1 proportions) was conducted enabling the unambiguous detection, in very soft conditions, of the mixture composed of the three silver adducts $[Ag@D_3\text{-}\mathbf{42}]^+$/$[2Ag@D_3\text{-}\mathbf{42}]^{2+}$/$[3Ag@D_3\text{-}\mathbf{42}]^{3+}$. The relative stabilities evaluated by the abundance ratio measured from the mixture (11.2:100:3.8) indicated that the bis-cationic $[2Ag@D_3\text{-}\mathbf{42}]^{2+}$ complex is the most stable complex in the gas phase. This preference may be explained by the existence of a more compact and better adjusted conformation for bis-cationic $[2Ag@D_3\text{-}\mathbf{42}]^{2+}$ than for its mono- and tris-cationic analogues. Theoretical calculations confirmed the bis-η^2-type coordination mode of Ag(I) toward the outer phenyl rings.

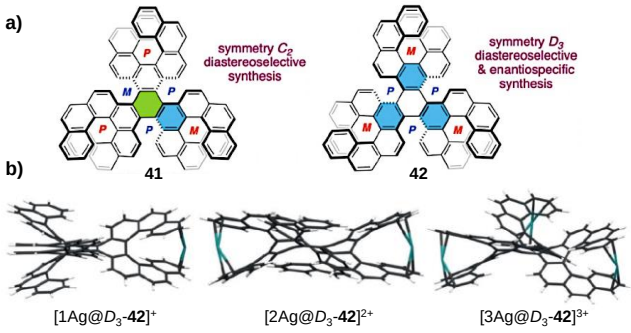

Figure 12. Chemical structures of multihelicenic diastereomeric systems **41** and **42**. b) Computationally optimized structures of the most stable mono, bis, and triscationic Ag^+ complexes of D_3-**42** (DFT, wB97XD/ Def2TZVP//wB97XD/Def2SVP, gas phase). Reproduced with permission from ref. [52]. Copyright 2020, Wiley-VCH.

3.2. Multihelicenic metal-alkynyl complexes

3.2.1. Helicene-ethynyl-gold complexes

Another approach to organometallic complexes relies on the ability of metal centers to coordinate through the formation of metal-alkynyl bonds, readily created from the corresponding terminal alkyne derivative under basic conditions. Hence, starting from a bimetallic precursor and a helicenic acetylide derivative, bishelicenic organometallic species could be readily obtained by our group: 2-ethynyl[4]helicene **43** and 2-ethynyl[6]helicene **44** in combination with bis-phosphole d^{10} gold(I) complexes **P1** or **P2** gave bimetallic [4]- and [6]-helicene-alkynyl-phoshole gold(I) complexes **45**,**46** and **47**,**48**. In **45** and **46**, both Au(I) centers are brought close to each other, promoting aurophilic interactions whereas in **47** and **48**, the two Au^I centers are too far away to display any aurophilic interactions[54] thus leading to different electronic behaviors.[55] Note that **45** and **47** are not chiral due to rapid interconversion of the [4]helicenic units in solution. X-ray crystallography of **45** revealed that the two ethynyl helicenes units are far from each other to display any specific interactions (π-π or CH-π interactions). Complexes **46** and **48** were synthesized from the corresponding enantiopure *P*- and *M*-**44** and investigation of the chiroptical properties showed that the "Z-shape" complex **48** without aurophilic interactions displayed a higher ECD response than the "U-shape" complex **46** with Au^I-Au^I interactions, reinforcing the properties-structures relationship: bringing the helicenic moieties close together *via* non-specific interactions decreases the chiroptical response. These observations were confirmed by the molar rotation values (**46**: ± 35290; **48**: ± 43400) even comparing with the helicenic ligand **44** (± 11030) or the mono helicenic complex derivative **49** (± 21340). Theoretical calculations supported these results by highlighting the efficiency of LLCT-type transitions from the two helicenic moieties to the π-conjugated phosphole scaffold to be involved in the chiroptical properties (see HOMO-to-LUMO on Figure 13d) along with the influence of the two helical units interacting through space.

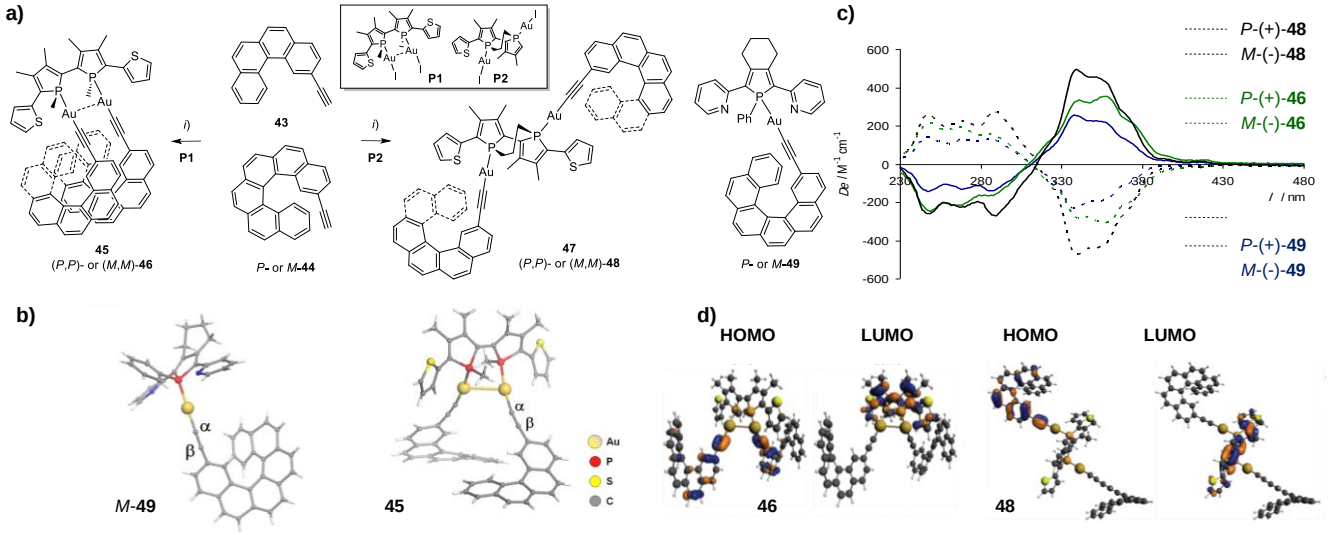

Figure 13. a) Synthesis of monometallic gold(I)-alkynyl-helicene complex **49** and bimetallic gold(I)-alkynyl-helicene assemblies featuring the presence (**45**,**46)** or absence (**47**,**48)** of aurophillic intramolecular interactions. *i*) Bis-phosphole gold(I) iodide **P1** or **P2**, NaOMe, CH_2Cl_2, MeOH, Ar. b) X-ray crystallographic structures of complex **49** and of model assembly **45** with two [4]helicene units and displaying Au(I)-Au(I) interaction. c) ECD spectra (5 10^{-5} M in CH_2Cl_2) of monometallic complex *P* and *M*-**49** (blue) and of *P* and *M* enantiomeric bimetallic bis-assemblies **46** (green) and **48** (black). Plain lines for *P* enantiomers and dotted lines for *M* enantiomers. d) Helicene-centered HOMOs and biphosphole-centered LUMOs of complexes **46** and **48** (in one selected geometry). Adapted with permission from ref [55]. Copyright 2016, Wiley-VCH.

3.2.2. Ruthenium-ethynyl complexes with helicene and DTE moieties

Through the next example, we show that complexity can be introduced in chiral organometallic switching systems by combining two different and complementary input stimuli (redox potential and light). In 2018, Rigaut, Crassous, *et al.* reported organometallic complex (*P*,*P*)-**50o** acting as a dual redox- and photo-responsive bis-helicene derivative prepared by decorating a dithienylethene (DTE) with two ethynyl-ruthenium-ethynyl-carbo[6]helicene units (Figure 14a).[56] Upon action of a 365 nm irradiation, enantiopure open form (*P*,*P*)-**50o** was transformed into closed form **50c** as a mixture of diastereomers [(*P*,*P*,*R*,*R*) and (*P*,*P*,*S*,*S*)-**50c**], *i.e.* in a non-stereoselective way, due to the newly formed chiral centers at α-positions of the two thiophenes. The conrotatory ring closing reaction can indeed generate both (*R*,*R*) and (*S*,*S*) configurations and thus form a pair of diastereomers (*P*,*P*,*R*,*R*)- and (*P*,*P*,*S*,*S*)-**50c** when starting from the enantiopure (*P*,*P*)-**50o**. The photochemical process was followed by UV-vis and ECD spectroscopies and despite the presence of two diastereomers for **50c**, a visible and ECD-active band appeared around 720 nm ($\Delta\varepsilon$~+6 L·mol^{-1}·cm^{-1}, see inset Figure 14b) evidencing the π-conjugation pathway through the whole molecule, *i.e.* between the two helicene units via the DTE chromophore. Complex **50c** could in its turn be opened back to (*P*,*P*)-**50o** by using a 650 nm light. In parallel, upon action of a +0.7 V (vs. Ag) potential, (*P*,*P*)-**50o** could be doubly oxidized to (*P*,*P*)-[**50o**]$^{2+}$ which appeared unstable and spontaneously transformed to the closed form (*P*,*P*)-[**50c**]$^{2+}$ (see ECD fingerprint on Figure 14c). Then upon action of a -0.6 V potential, this species was reduced to (*P*,*P*)-**50c** which in its turn could be reopened back to (*P*,*P*)-**50o** through light, thus giving access to an irreversible 3-states cycle, as clearly depicted in the UV-vis-near IR spectrum on Figure 14d.

Based on its photochromic and electrochromic properties, complex **50o** could be used as a logic gate.[57] Indeed, the circular dichroism ($\Delta\varepsilon$) of this molecule at 679 nm could be used as output read-out values, with the absence (presence) of ECD signal defined “0” (“1”) output value. Two inputs could be implemented: (no) irradiation at 365 nm corresponded to (“0”) “1” in the photochemical process. External redox potential of +0.7 V then of −0.6 V *vs*. Ag wire corresponds to “1” in E, otherwise “0” with no redox stimulus. As a result described in Figure 14e, the system can be described as an “OR” logic gate (i.e. with a “1” output value whenever we apply either a redox or a wavelength stimulus). Therefore, this chiral bis-helicenic system enabled to obtain a new type of chiroptical switch. Note that similar DTE system but grafted with only one ethynyl-Ru-ethynyl-helicene unit gave a 'NOR' logic gate instead, thus highlighting the complementarity of having either one or two helicenic units.

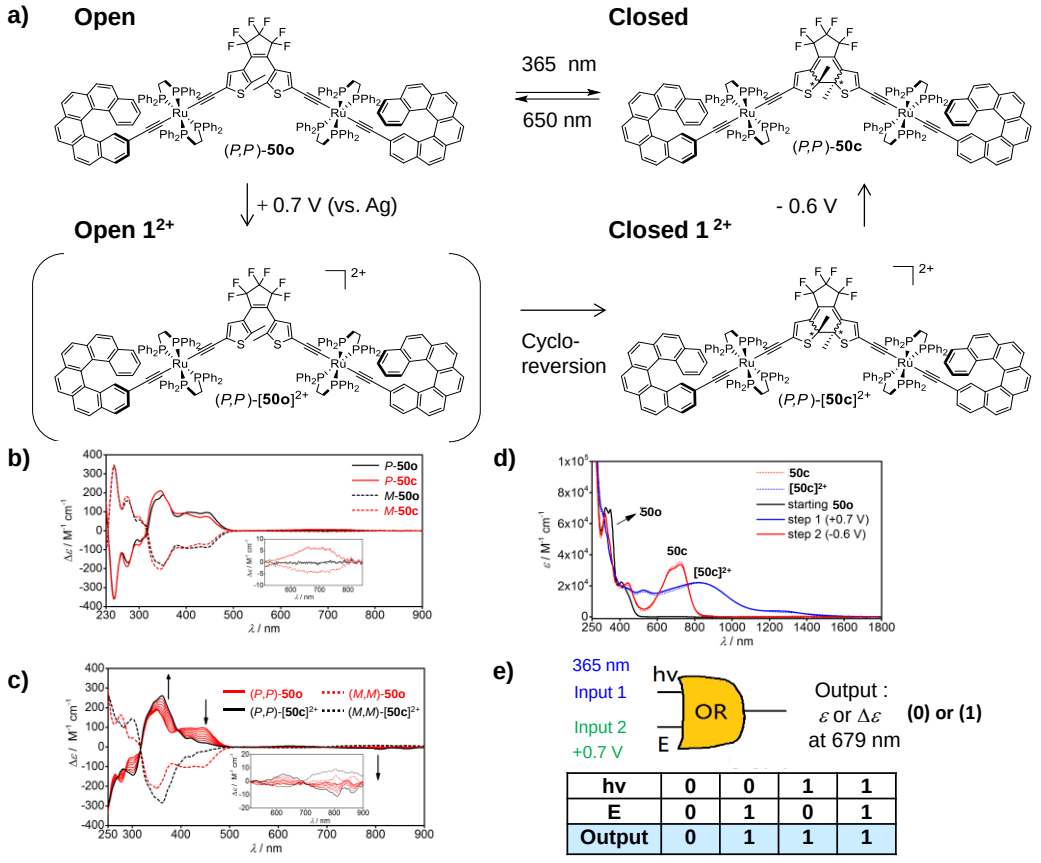

Figure 14. a) DTE-based bis-helicene-ethynyl-Ru complex **50o/50c** and their bis-oxidized forms [**50o**]$^{2+}$/[**50c**]$^{2+}$, and the full cycle of oxidation (+0.7V) / spontaneous ring closure (cycloreversion) / reduction (-0.6V) / ring opening (650 nm). b) Modification of ECD spectra upon DTE ring closure (**50c** *vs.* **50o**) and c) upon oxidation ([**50c**]$^{2+}$ *vs.* **50o**). d) Switching process between three states *P*-**50c**/*IP*-([**50c**]$^{2+}$/*IP*-**50o** monitored by UV/vis. e) 'OR' logic gate obtained by fixing light and redox potential as input stimuli and reading out the response at 679 nm (either absorption or ECD).

3.3. Multihelicenic cyclometallated complexes

To construct multihelicenic organometallic frameworks by incorporating metallic ions with a π-helical backbone, the use of C-H *ortho*-metallation has proved to be a useful synthetic tool. Indeed, such methodology has been firstly exemplified by our group in 2010, with bis-[6]helicenic-bis-platinum(II)-μ-chloro bridged dimer **52** prepared by treatment at high temperature of 2-(benzophenanthrenyl)pyridine **51** with K_2PtCl_4 as a metallic source (Figure 15).[58] The cycloplatination provides a platinacycle embedded within a fully *ortho*-fused system which possess two additional rings as compared to the starting proligand, thus enabling to go from a labile [4]helicene to a configurationally stable [6]helicene. Such assembly is named metallahelicene since the metal is inserted within the π-conjugated system. The cleavage of **52** upon reaction with acetylacetone furnished the monocycloplatinated complex **53** possessing one helicene unit. The square planar Pt(II) center being not a stereogenic element, the number of stereoisomers is low when associated with helicenic ligands, *i.e.* (*P*,*P*), (*M*,*M*)- **52**^{1} and *meso* compound (*P*,*M*)-**52**^{2} for the dimer **52** and *P* or *M* for monomer **53**. Using a similar approach, a tetra-[6]helicenic-bis-iridium(III)-μ-chloro bridged dimeric mixture **54** was prepared by action at high temperature of $IrCl_3$ on **51** (Figure 15), which in its turn furnished the cycloiridiated complex **55** possessing two helicenic units by reaction with acetylacetone in the presence of a base.[58] Compared to platinum, iridium chemistry appears much more complex. Indeed, complex **54** possesses four helicenic ligands and two octahedral Ir(III) center connected to each other through μ-chloro bridges. The helical ligands and the iridium centers being both stereogenic (respectively, *P/M, Δ/Λ, fac/mer*),[59] mixtures of stereoisomers were obtained for **54** and **55**. Up to 64 (2^6) stereoisomers for **54** and up to 8 (2^3) stereoisomers for **55** could be potentially statistically obtained starting from an achiral ligand **51.** However, only one enantiomeric pair was obtained for **54**, after purification by crystallization, which was identified as (*P,P,P,P,mer,Λ,Λ,*)/(*M,M,M,M,mer,Δ,Δ*) stereoisomer, while purification by silica gel column chromatography yielded two enantiomeric pairs of diastereoisomers, namely (*P,P,mer,Δ*)/(*M,M,mer,Λ*)-**55**^{1} and (*P,M,mer,Δ*)/(*P,M,mer,Λ*)-**55**^{2} as observed by X-ray crystallographic analysis (see Figure 15).

In 2011, it was shown that when bis-platinum(II)-μ-chloro bridged dimer **52** was put in the presence of silver benzoate, a mixture of two species was obtained in a 9:1 ratio and with 57% yield. NMR analysis revealed that the major complex **56a** had a C_1 symmetry while the minor derivative had a C_2 symmetry **56b** (Figure 16a). They were both further characterized as superimposed μ^2-benzoato bridged platina-[6]helicenes assembled in *anti*-conformation for the (*C*,*N*) briding ligands with the two Pt(III) centers being inserted in the helical cores and linked through a Pt(III)-Pt(III) bond.[60] The chloro ligands complete the coordination sphere of each Pt center. X-ray crystallography confirmed the single bond between the two Pt(III) centers along with the heterochiral and the homochiral nature for **56a** and **56b** respectively, that fully matched the NMR analysis (Figure 16c). Quite interestingly, while heated in toluene at 80°C for 3 days under inert atmosphere, the mixture 9:1 **56a/56b** could be smoothly converted into pure **56b** with the two helices displaying now the same handedness, as confirmed by X-ray crystallography in line with the NMR analysis. The feasibility of this transformation was supported by DFT calculations that evaluated the energetic gap between the two isomers between 0.4 and 0.6 kcal/mol depending on the level of theory used to describe the system in favour of **56b**, thus suggesting that the heterochiral (homochiral) corresponds to the kinetic (thermodynamic) product. In order to investigate the chiroptical properties of such bis-helicenic systems, both enantiomers of **56b** were synthesized following a slightly modified route: enantiopure Pt^{II} complex **57**, bearing dmso and chloro ancillary ligands and obtained from the *ortho*-metallation of **51** and further separated by chiral HPLC separation, was put in reaction with silver benzoate following the same procedure as previously and enabled the formation of the desired enantiopure homochiral complex (Figure 16b). **56b** enantiomers display intense ECD spectra in comparison with monohelicenic **57** (Figure 16d) and a huge molar rotation (± 28200) that is at least 3 times higher than other mono-platina-[6]helicenes reported in the literature (± 7060-8170), emphasizing the interest to combine several helicenic systems in order to enhance the chiroptical properties. These properties were explained by the efficient conjugation between both helical moiety through the Pt(III)-Pt(III) bond (σ–π conjugation, as clearly shown in the HOMO and LUMO on Figure 16e.[60,61]

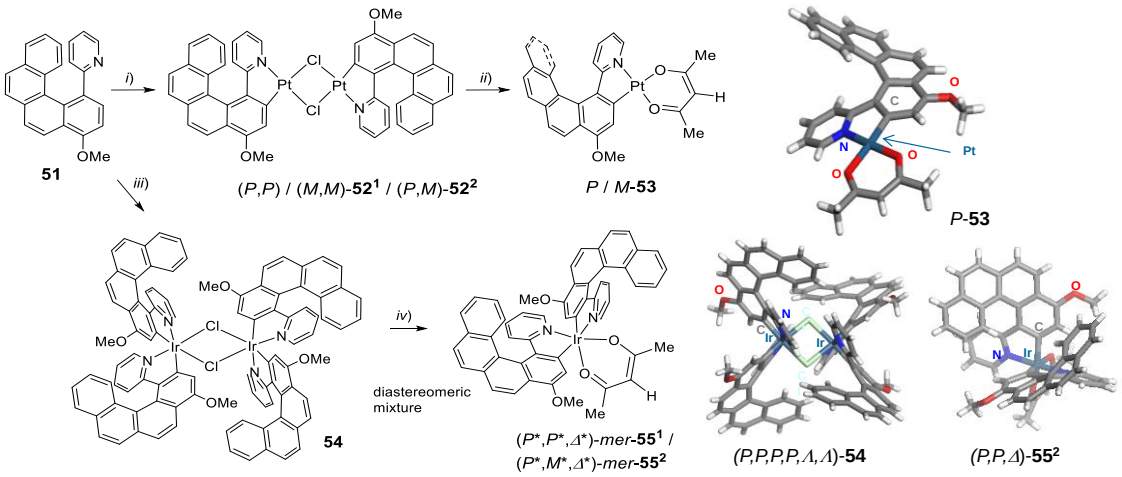

Figure 15. Synthesis of bis-platina[6]helicenes **52**^{1,2} and tetra-irida[6]helicenic diastereomeric mixture **54** together with mono-platina[6]helicene **53** and bis-irida[6]helicenes **55**^{1,2}. *i*) K_2PtCl_4, ethoxyethanol, H_2O, reflux, 16 hrs; *ii*) AcacH, Na_2CO_3, ethoxyethanol, reflux, 2 hrs, 52%; *iii*) $IrCl_3$, $P(OMe)_3$, 75 °C, one night; *iv*)

10.1002/anie.202004361

AcacH, K_2CO_3, 85°C, 2 hrs, 22%. X-ray crystallographic structures of *P*-**53**, homochiral (*P*,*P*,*P*,*P*,*Δ*,*Δ*)-**54** and (*P*,*P*,*Δ*)-**55²**. Adapted with permission from ref. [58]. Copyright 2010, Wiley-VCH.

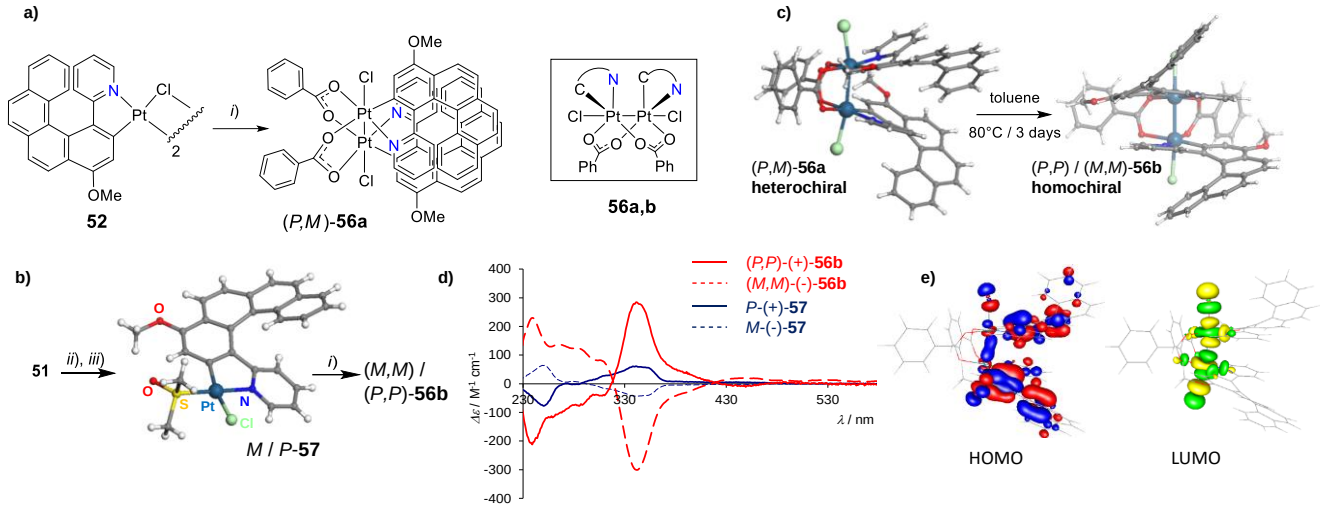

Figure 16. a) Synthesis of homochiral and heterochiral bis-(Pt[III][6]helicene) (**56a,b**) assemblies; *i*) $PhCO_2Ag$, $CHCl_3$/THF, rt, 12 hrs, Ar. b) Synthesis and X-ray structure of mono-Pt[II][6]helicene **57**. *ii*) $Pt(dmso)_2Cl_2$, toluene, 110°C, Ar, 16 hrs, 85%; *iii*) HPLC separation. c) X-ray structures and isomerization process of heterochiral **56a** to homochiral **56b**. d) ECD spectra of homochiral bimetallic **56b** compared to monometallic **57** pure enantiomers. e) FMOs of complex **56b**. Adapted with permission from ref. [60]. Copyright 2011, ACS.

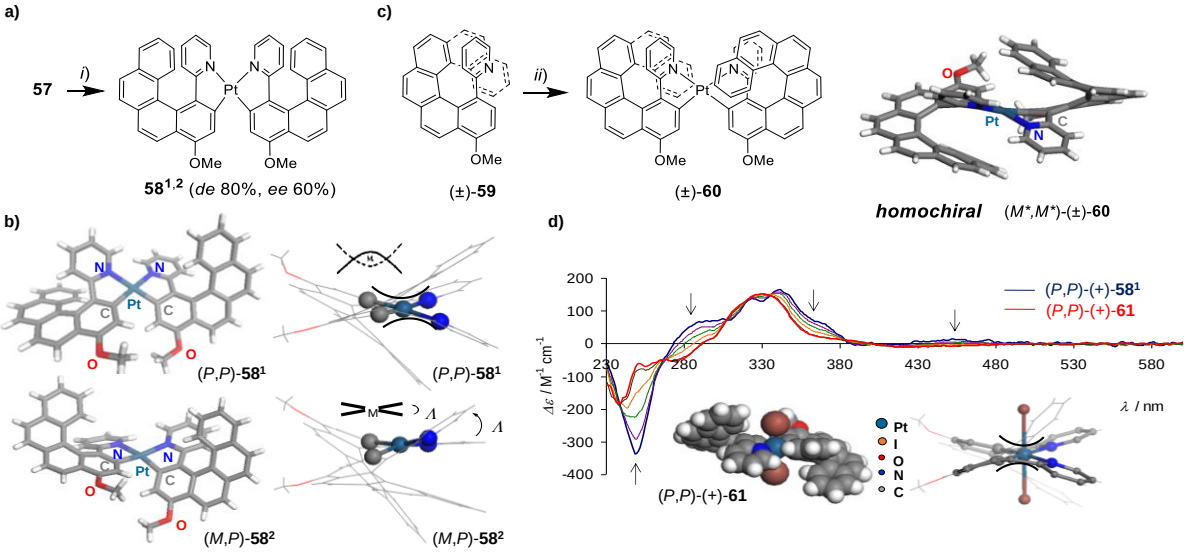

Figure 17. a) Synthesis of mono-platina-bis[6]helicenes **58¹**/**58²**. *i*) $AgBF_4$, acetone, Ar, then **51**, Na_2CO_3, toluene, 110°C, 10 min, 63%. b) X-ray crystallographic structures of homochiral (*P*,*P*)-**58¹** and heterochiral (*M*,*P*)-**58²**. Bowlike and *Λ* geometries around the Pt[II] center in **58¹** and **58²** respectively. c) Synthesis and X-ray structure of mono-platina-bis[8]helicene (*M**,*M**)-**60**; *ii*) $Pt(dmso)_2Cl_2$, Na_2CO_3, xylene, reflux, 5%. d) X-ray structure of diiodo complex (*P*,*P*)-**61** and addition of iodine to (*P*,*P*)-**58¹** followed by ECD spectroscopy. Adapted with permission from ref. [62]. Copyright 2013, Wiley-VCH.

Enantiopure **57** was also used as precursor for the construction of monometallic mono-platina-bis[6]helicene **58** *via* cationization of the Pt[II] center and subsequent *ortho*-metallation in presence of achiral **51**.[62] NMR studies and HPLC analysis after the *ortho*-metallation process revealed the diastereoselective/enantioselective nature of the reaction allowing to isolate homochiral **58¹** in a 90:10 ratio in comparison to the meso compound **58²** (*i.e.* 80% of diastereomeric excess, *de*) and with 60% *ee* after purification. The rare selectivity observed during the cycloplatination has been explained by the combination of **51**'s flexible scaffold along with the efficient transfer of chirality enabled by the chiral mono platina-[6]helicene precursor **57**. Both homochiral and heterochiral **58¹,²** display *cis* conformation for the phenyl pyridine-like ligands but notably, the geometry around the metal centers is different depending the isomer: **58¹** possesses a bow-like shape arrangement whereas **58²** shows a *Δ*/*Λ* stereochemistry. This is reminiscent of seminal work from von Zelewsky.[63] Enantiopure samples of **58¹** were obtained by chiral HPLC and the chiroptical properties were investigated. Bis-helicenic complex **58¹** displays highly intense

ECD signature along with a high molar rotation (± 18460) which is twice that of mono-platinahelicenes.[58] Another interesting feature of **58[1]** is its ability for iodine sensing, efficiently probed by circular dichroism and related to the properties of the Pt(II) center that could be oxidized into Pt(IV) (see ECD in Figure 17d). Finally, starting from [6]helicene-pyridine derivative **59**, the [8]helicene analogue of **58[1]**, that is **60**, bearing two homochiral platina[8]helicenes sharing the same Pt(II) center was successfully obtained by the same method (see synthesis and X-ray structure of the (*M*,*M*) isomer on Figure 17c). Despite the low yield of the transformation (5%), this last example illustrated the versatility of the *ortho*-metallation in order to assemble several π-conjugated ligands and access derivatives with higher helicity.[62]

Summary and outlook

In conclusion, considering the huge amount of organic architectures chemists can prepare together with the multitude of metallic centers available, an infinity of multihelicenic metallo-based structures can be targeted. To this aim, we have at disposal several strategies, *i.e.* either using metallic ions as connectors for monohelicenic ligands or first preparing organic multihelicenic ligands and make them react with metallic ions, even further assembling these multihelicenic building blocks into more sophisticated systems. This strategy uses the rich toolbox of interactions such as interactions through metals (metallophilic interactions, covalent metal-metal bonds), through van der Waals interactions between ligands, through specific π–π or CH-π interactions, etc. Such strategy enables to combine sophisticated helical ligands and metal complexes in which the very strong chiroptical activity originates from the several helicene units in the assembly and from additional electronic transitions mainly originating from charge transfers between metal and ligand, or between ligands only. Racemization processes and stereochemical fates upon coordination are important aspects to control. Luminescence properties and CPL activity may also appear or be modified upon introduction of metallic ions into helicenic architectures, thus yielding CPL tuning. As for organometallic multihelicenic species, the M-C bonds enable to strongly modify the interaction between metal and helical ligands, resulting in strong changes in the redox activity and strong impact of the chiroptical activity. Elaborated chiral architectures or metallo-organic frameworks with controlled topologies may thus be prepared and utilized in many fields such as chiral sensing and host-guest enantioselective recognition, enantioselective catalysis, development of chiral materials like CP-emitters, conductive films, NLO-active fibers, etc. Finally, this strategy enables to introduce efficient chiroptical switching processes and future directions in this field may consist in obtaining controlled directional motions within polyhelicenic chiral systems. Overall, the concomitant evolution of fully organic as well as metal-based multihelicenic is thus a great opportunity for scientists to discover new frontiers in chemistry and chiral materials science. In summary, metallic systems may lead to different or complementary features and applications as compared to organic ones. There are numerous potentialities of such systems combining chirality, π-conjugated units and metallic ions. The added values are related to and depend on each metal selected (providing either emission, redox activity, recognition, …). Regarding future works, this topic is still at its infancy and many directions are open, for instance in chiral catalysts, chiral coordination polymers, or chiral helicene-based metal-organic frameworks (MOFs).

Acknowledgements

We thank the Centre National de la Recherche Scientifique (CNRS) and the University of Rennes. This work was supported by the Agence Nationale de la Recherche (ANR-16-CE07-0019 “Hel-NHC” grant). R.R. Thanks Xunta de Galicia for a postdoctoral fellowship.

Keywords: multihelicenic complexes • coordination assemblies • organometallics • chirality • chiroptical activity

† These authors contributed equally.

[1] C.-F. Chen, Y. Shen, In *Helicene Chemistry: From Synthesis to Applications*; Springer Berlin Heidelberg: Berlin, Heidelberg, 2017.
[2] Y. Shen, C.-F. Chen, *Chem. Rev.* **2011**, *111*, 1463-1535.
[3] M. Gingras, *Chem. Soc. Rev.* **2013**, *42*, 1007-1050.
[4] K. Dhbaibi, L. Favereau, J. Crassous, *Chem. Rev.* **2019**, *119*, 8846-8953.
[5] T. Verbiest, S. Van Elshocht, M. Kauranen, L. Hellemans, J. Snauwaert, C. Nuckolls, T. J. Katz, A. Persoons, *Science* **1998**, *282*, 913-915.
[6] S. Guy, B. Baguenard, A. Bensalah-Ledoux, D. Hadiouche, L. Guy, *ACS Photonics* **2017**, *4*, 2916-2922.
[7] H. Isla, J. Crassous, *C. R. Chimie* **2016**, *19*, 39-49.
[8] T. R. Kelly, X. Cai, F. Damkaci, S. B. Panicker, B. Tu, S. M. Bushell, I. Cornella, M. J. Piggott, R. Salives, M. Cavero, Y. Zhao, S. Jasmin, *J. Am. Chem. Soc.* **2007**, *129*, 376-386.
[9] D.-W. Zhang, M. Li, C.-F. Chen, *Chem. Soc. Rev.* **2020**, *49*, 1331-1343.
[10] Y. Yang, R. C. da Costa, M. J. Fuchter, A. J. Campbell, *Nat. Photonics* **2013**, *7*, 634-638.
[11] V. Kiran, S. P. Mathew, S. R. Cohen, I. Hernandez Delgado, J. Lacour, R. Naaman, *Adv. Mater.* **2016**, *28*, 1957-1962.
[12] C. Li, Y. Yang, Q. Miao, *Chem. Asian J.* **2018**, *13*, 884-894.
[13] K. Kato, Y. Segawa, K. Itami, *Synlett* **2019**, *30*, 370-377.
[14] N. Saleh, C. Shen, J. Crassous, *Chem. Sci*. **2014**, *5*, 3680-3694
[15] J.-K. Ou-Yang, J. Crassous, *Coord. Chem. Rev.* **2018**, *376*, 533-547.
[16] C. Elschenbroich, *Organometallics*, Wiley VCH, 2006.
[17] H. Le Bozec, V. Guerchais, *Molecular Organometallic Materials for Optics: 28 (Topics in Organometallic Chemistry)*, Springer Berlin Heidelberg, 2009.
[18] J. -M. Lehn, *Supramolecular Chemistry: Concepts and Perspectives*, VCH, Weinheim, 1995.
[19] Z. Zhou, R. K. Kawade, Z. Wei, F. Kuriakose, Ö. Üngör, M. Jo, M. Shatruk, R. Gershoni-Poranne, M. A. Petrukhina, I. V. Alabugin, *Angew. Chem. Int. Ed.* **2020**, *59*, 1256-1262.
[20] S. I. Weissman, R. Chang, *J. Am. Chem. Soc.* **1972**, *94*, 8683-8685.
[21] M. J. Narcis, N. Takenaja, *Eur. J. Org. Chem*. **2014**, 21-34.
[22] Y. Yang, R. C. da Costa, M. J. Fuchter, A. J. Campbell, *Nat. Photonics*, *2013*, 7, 634-638.
[23] J. Misek, F. Teply, I. G. Stara, M. Tichy, D. Saman, I. Cisarova, P. Vojtisek, I. Stary, *Angew. Chem. Int. Ed.* **2008**, *47*, 3188-3191.
[24] J. Misek, M. Tichy, I. G. Stara, I. Stary, D. Schroeder, *Collect. Czech. Chem. Commun*. **2009**, *74*, 323-333.
[25] I. Alkorta, F. Blanco, J. Elguero, D. Schröder, *Tetrahedron: Asymmetry* **2010**, *21*, 962-968.
[26] Y. Sanogo, P. Aillard, P. Retailleau, A. Voituriez, A. Marinetti, *Chirality*, **2019**, *31*, 561-567.
[27] M. El Sayed Moussa, K. Guillois, W. Shen, R. Réau, J. Crassous, C. Lescop, *Chem. Eur. J.* **2014**, *20*, 14853-14867.
[28] S. D. Dreher, T. J. Katz, K.-C. Lam, A. L. Rheingold, *J. Org. Chem*. **2000**, *65,* 815-822.
[29] D. Nakano, M. Yamaguchi, *Tetrahedron Lett.* 2003, *44,* 4969-4971.
[30] H. Okubo, M. Yamaguchi, C. Kabuto, *J. Org. Chem*. **1998**, *63*, 9500-9509.

[31] H. Isla, N. Saleh, J.-K. Ou-Yang, K. Dhbaibi, M. Jean, M. Dziurka, L. Favereau, N. Vanthuyne, L. Toupet, B. Jamoussi, N. Srebro-Hooper, J. Crassous, *J. Org. Chem*, **2019**, *84*, 5383-5393.

[32] W. Shen, S. Graule, J. Crassous, C. Lescop, H. Gornitzka, R. Réau, *Chem. Comm.* **2008**, 850-852.

[33] J. Crassous, R. Réau, *Dalton Trans.* **2008**, 6865-6876.

[34] S. Graule, M. Rudolph, N. Vanthuyne, J. Autschbach, C. Roussel, J. Crassous, R. Réau, *J. Am. Chem. Soc.* **2009**, *131*, 3183-3185.

[35] S. Graule, M. Rudolph, W. Shen, C. Lescop, J. A. G. Williams, J. Autschbach, J. Crassous, R. Réau. *Chem. Eur. J.*, **2011**, *17*, 1337-1351.

[36] T. R. Schulte, J. J. Holtein, G. H. Clever, *Angew. Chem.* **2019**, *58*, 5562-5566.

[37] A. Petitjean, R. G. Khoury, N. Kyritsakas, J.-M. Lehn, *J. Am. Chem. Soc.* **2004**, *126*, 6637-6647.

[38] H. Isla, M. Srebro-Hooper, M. Jean, N. Vanthuyne, T. Roisnel, J. L. Lunkley, G. Muller, J. A. G. Williams, J. Autschbach, J. Crassous, *Chem. Commun.* **2016**, *52*, 5932-5935.

[39] A. I. Aranda Perez, T. Biet, S. Graule, T. Agou, C. Lescop, N. R. Branda, J. Crassous, R. Réau, *Chem. Eur. J,* **2011**, *17*, 1337-1351.

[40] V. Vreshch, M. El Sayed Moussa, B. Nohra, M. Srebro, N. Vanthuyne, C. Roussel, J. Autschbach, J. Crassous, C. Lescop, R. Réau, *Angew. Chem. Int. Ed*. **2013**, *52*, 1968-1972.

[41] J. M. Fox, T. J. Katz, S. Van Elshocht, T. Verbiest, M. Kauranen, A. Persoons, T. Thongpanchang, T. Krauss, L. Brus, *J. Am. Chem. Soc*. **1999**, *121*, 3453-3459.

[42] Y. Dai, T. J. Katz, D. A. Nichols, *Angew. Chem. Int. Ed.* **1996**, *35*, 2109-2111.

[43] Y. Dai, T. J. Katz, *J. Org. Chem.* **1997**, *62*, 1274-1285.

[44] A. Sudhakar, T. J. Katz, B.-W. Yang, *J. Am. Chem. Soc.* **1986**, *108*, 2790-2791.

[45] T. J. Katz, A. Sudhakar, M. F. Teasley, A. M. Gilbert, W. E. Geiger, M. P. Robben, M. Wuensch, M. D. Ward, *J. Am. Chem. Soc*. **1993**, *115*, 3182-3198.

[46] A. M. Gilbert, T. J. Katz, W. E. Geiger, M. P. Robben, A. L. Rheingold, *J. Am. Chem. Soc*. **1993**, *115*, 3199-3211.

[47] T. J. Katz, W. Slusarek, *J. Am. Chem. Soc*. **1979**, *101*, 4259-4267.

[48] A. Sudhakar, T. J. Katz, *J. Am. Chem. Soc*. **1986**, *108*, 179-181.

[49] J. C. Dewan, *Organometallics* **1983**, *2*, 83-88.

[50] F. Pammer, Y. Sun, M. Pagels, D. Weismann, H. Sitzmann, W. R. Thiel, *Angew. Chem. Int. Ed*. **2008**, *47*, 3271-3274.

[51] M. Akiyama, K. Nozaki, *Angew. Chem. Int. Ed.* **2017**, *56*, 2040-2044.

[52] M. Roy, V. Berezhnaia, M. Villa, N. Vanthuyne, M. Giorgi, J.-V. Naubron, S. Poyer, V. Monnier, L. Charles, Y. Carissan, D. Hagebaum-Reignier, J. Rodriguez, M. Gingras, Y. Coquerel, *Angew. Chem. Int. Ed.* **2020**, *59*, 3264-3271.

[53] M. J. Fuchter, J. Schaefer, D. K. Judge, B. Wardzinski, M. Weimar, I. Krossing, *Dalton Trans.* **2012**, *41*, 8238-8241.

[54] H. Chen, W. Delaunay, L. Yu, D. Joly, Z. Wang, J. Li, Z. Wang, C. Lescop, D. Tondelier, B. Geffroy, et al., *Angew. Chem. Int. Ed.* **2012**, *51*, 214-217.

[55] M. El Sayed Moussa, H. Chen, Z. Wang, M. Srebro-Hooper, N. Vanthuyne, S. Chevance, C. Roussel, J. A. G. Williams, J. Autschbach, R. Réau, Z. Duan, C. Lescop, J. Crassous, *Chem. Eur. J.* **2016**, *22*, 6075-6086.

[56] C. Shen, X. He, L. Toupet, L. Norel, S. Rigaut, J. Crassous, *Organometallics* **2018**, *37*, 697-705.

[57] J. Andreasson, U. Pischel, *Chem. Soc. Rev.* **2010** *39*, 174-188.

[58] L. Norel, M. Rudolph, N. Vanthuyne, J. A. G. Williams, C. Lescop, C. Roussel, J. Autschbach, J. Crassous, R. Réau, *Angew. Chem.* **2010**, *122*, 103-106.

[59] A. Von Zelewsky, *Stereochemistry of Coordination Compounds*, J. & Wiley & Sons, Chichester, **1996**.

[60] E. Anger, M. Rudolph, C. Shen, N. Vanthuyne, L. Toupet, C. Roussel, J. Autschbach, J. Crassous, R. Réau, *J. Am. Chem. Soc.* **2011**, *133*, 3800-3803.

[61] E. Anger, M. Rudolph, L. Norel, S. Zrig, C. Shen, N. Vanthuyne, L. Toupet, J. A. G. Williams, C. Roussel, J. Autschbach, J. Crassous, R. Réau, *Chem. Eur. J.*, **2011**, *17,* 14178-14198.

[62] C. Shen, E. Anger, M. Srebro, N. Vanthuyne, L. Toupet, C. Roussel, J. Autschbach, R. Réau, J. Crassous, *Chem. Eur. J.* **2013**, *19*, 16722-16728.

[63] L. Chassot, E. Muller, A. Von Zelewsky, *Inorg. Chem.* **1984**, *23*, 4249-4253.

10.1002/anie.202004361

WILEY-VCH

MINIREVIEW

Entry for the Table of Contents

Insert graphic for Table of Contents here. ((Please ensure your graphic is in **one** of following formats))

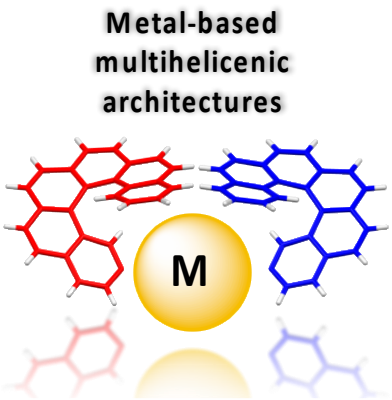

Let's assemble them all! Using either coordination chemistry or organometallic approaches, diverse metallo-multihelicenic systems have been designed. The association of helically chiral π-conjugated ligands in close proximity with metal centers resulted in sophisticated architectures exhibiting new properties compared with the corresponding monohelicenic structures.

Institute and/or researcher Twitter usernames: @chimie_ISCR, @EGA_chem, @ChiralMat, @JeanneCrassous